IEEE Access
Multidisciplinary : Rapid Review : Open Access Journal

Received 2 March 2025, accepted 1 April 2025, date of publication 4 April 2025, date of current version 17 April 2025.

Digital Object Identifier 10.1109/ACCESS.2025.3557937

RESEARCH ARTICLE

Comprehensive Review of Control Techniques for Various Mechanisms of Parallel Robots

SHAYMAA MAHMOOD MAHDI[1], **AHMED I. ABDULKAREEM**[1], **AMJAD JALEEL HUMAIDI**[1], **AMMAR K. AL MHDAWI**[2], **AND HAMED AL-RAWESHIDY**[3], **(Senior Member, IEEE)**

[1]Department of Control and Systems Engineering, University of Technology-Iraq, Baghdad 10066, Iraq
[2]School of Engineering and Sustainable Development, Electrical, Electronics and Mechatronics Group, De Montfort University, LE1 9BH Leicester, U.K.
[3]Department of Electronic and Electrical Engineering, Brunel University of London, UB8 3PH Uxbridge, U.K.

Corresponding author: Hamed Al-Raweshidy (hamed.al-raweshidy@brunel.ac.uk)

ABSTRACT This study provides a literature review of control schemes associated with parallel robots. Various types of parallel robots have been discussed, including the Delta Robot, 2 DOF Parallel Robot, 3 DOF Parallel Robot, 4 DOF Parallel Robot, the R4 Redundantly Parallel Robot, the 5R Parallel Robot, 6 DOF Parallel Robot (Hexa Robot), Cable-Driven Parallel Robot, and Parallel Quadruped Robot. Additionally, an overview of the control structuring within these systems has been provided. This study covers the developments occurring between 2008 and 2024. These controllers are PI Control, PID Control, Genetic Algorithm Optimized PID Control, Extended PD Control, Augmented Nonlinear PD Control, Model-Based PD Control, Synchronous PD Control Based on a Time-Delay Estimator, Identification–Based Control, Image-Based Control, Lagrangian Formulation-Based Control, Observers–Based Control, Optimal PID Control, Anti-Windup Based PID Control, Model-Based Control, PLC–Based Control Architecture, Feedback PID Control, and Computed Torque Control, Hedge Algebras Control, B-Spline Neural Network Control, Fuzzy Logic Control, Model-Based control, Cooperative Control, Brain Emotional Learning-Based Intelligent Control, Nonlinear Model Predictive Control, Fuzzy Logic–Based Sliding Surface Control, Fuzzy PID Control, Fuzzy- Based PID Control, Interval Type-2 Fuzzy Logic Control Fuzzy Logic based Neural Network Control, Nonlinear Model Predictive Control, Synchronous Sliding Mode Control, Observer–Based Sliding Mode Control, Sliding Mode–Based on Backstepping Control, LQ Optimal Control, Adaptive Fuzzy Control, Rise Feedback Control, Dual-Space Feedforward Control, Dual-Space Feedforward Control in the Cartesian Space, Dual-Space Feedforward Control, Dual Mode Adaptive Control, Nonlinear Dual Mode Adaptive Control, Optimized Fuzzy Adaptive PID Control, Adaptive Position-Force Control, Adaptive Admittance Control, and Robust Nonlinear Adaptive Control, Adaptive Robust Control, Adaptive Control, and Adaptive Terminal Sliding Mode Control, Robust control, fault tolerant controllers, and passivity control. The primary contribution is a literature review of control-based strategies for parallel robots, designed to inform those interested in control-oriented parallel robot research.

INDEX TERMS Parallel robot, delta robot, 9 types parallel robot, dynamic model of 9 types parallel robot, modern control, stability.

I. INTRODUCTION

Parallel robots, also referred to as parallel kinematic machines (PKM) or parallel manipulators, assert control over the motion of their end-effectors through a minimum of two kinematic chains extending from the end-effector to the fixed base. The first parallel robot (PR) was invented by James E. Gwinnet, in 1928 [1].

The mechanism of a parallel robot is designed as a closed-loop system with an end-effector (or mobile platform) with more than one degree of freedom (DOFs) and a fixed base. It is linked by independent kinematic chains (or legs), each composed of links and joints. Actuation is achieved through simple actuators placed in selected joints. Parallel

The associate editor coordinating the review of this manuscript and approving it for publication was Nasim Ullah.

mechanisms, by allowing the load to be shared among actuators, demonstrate a remarkably high load-carrying capacity. They are also known for their precision, rigidity, and ability to manipulate large loads, making them a reliable choice in the field of robotics [2].

Parallel robots are appealing for various applications because the load they handle is distributed among multiple legs of the system. As a result, each kinematic chain bears only a portion of the total load, creating inherently more rigid robots. These architectures also enable a reduction in the mass of the movable links, as the actuators are primarily fixed on the base, and many legs experience tension/compression forces. Consequently, this allows the use of less powerful actuators, promising structures with high payload, dynamic capacities, and accuracy. Parallel robots, with their versatile capabilities, find extensive use across a wide range of applications. The applications encompass pick-and-place in the food and pharmaceutical industries, milling, motion simulators, precision measurement systems, haptic devices, medical environments, flight simulation, and accessing offshore structures. The PKMs consist of different elements such as [3]:

- The immovable part of the robot is known as the fixed base.
- The end-effector where it is usually mounted known as the (moving) platform.
- The robot legs, which are the kinematic chains, link the base to the platform, where it is generally a serial or tree-structured kinematic chain.

Many studies have reviewed and surveyed the control schemes and configuration of the parallel robot. In [4], Patel and George, presented a comparison between serial and parallel manipulators. The study meticulously classified various parallel manipulators emphasizing their practical applications in industry, space, medical science, and commercial usage. In [5], Arora and Aggarwal conducted a review that specifically focused on parallel robotic systems and their applications in the medical field, particularly in robot-assisted surgeries and corresponding technologies. In [6], Azar et al. explored various control approaches for parallel robot controllers. They identified two main control technique classes: model-free and dynamic control. In [7], Qian, et al. presented a review for historical development of Cable drive parallel robots (CDPRs), introducing several latest application cases. The study focused on the design, performance analysis, and control theory of CDPRs. The aim of this review research is to assist readers in obtaining a detailed and quick overview of the design and analysis of CDPRs. In [8], Ratiu and Anton presented the results of recent works covering different types of parallel robots, parallel kinematic machines, or hybrid parallel mechanisms. The review study introduced some basic terms and discussed the different terminologies and definitions related to this topic. Also, it compered the advantages and disadvantages of parallel robots versus serial robots. In [1], Deabs, et al. investigated the performances of different parallel-robot structures in terms of stiffness, size of work space, and control characteristics. It has shown that higher degrees of freedom parallel robots provide greater stiffness, wider workspace, and better controller workspace, while lower degrees of freedom parallel robots result in lower weight, fewer links and joints, and smaller workspace. In [9], Abarca and Elias comprehensively analyzed the researches in the sense of rehabilitation development, assistive technology, and humanoid robots. This review article focused on parallel robot designed to mimic duplicate the movements of human body joints with three degrees of freedom, encompassing the neck, shoulder, wrist, hip, and ankle. They discussed parallel robots' timelines and advancements. It covers technology readiness levels (TRLs), design, degrees of freedom, kinematics structure, workspace assessment, functional capabilities, performance evaluation methods, and material selection for parallel robotics development. In [10], Kelaiaia et al. provided a comprehensive overview of the various approaches used in the optimal design of PMs and the main challenges faced. They proposed technical solutions to address the issue of the optimal dimensional design of PMs and outlined a seven-stage optimal design methodology. Additionally, they demonstrated the methodology's application for a 5R parallel manipulator with two degrees of freedom. In [11], Russo et al. presented a review study for those who are interesting in technology and functionality characteristics of parallel robot. The study presented the modeling tools for parallel mechanisms, which can be used in optimization, development, and evaluation of machine tool evaluation focusing on dynamics, kinematic metrics, calibration and error analysis. The main advantages, disadvantages of parallel machine tools are summarized and the obstacles preventing the implementations of these systems are highlighted.

In spite of the above review literatures are very important and instructive; however they have focused either on reviewing of special purpose parallel robot like Delta parallel robot and Cable drive parallel robot, or reviewing on special applications such as pick and place, medical, human-robot collaboration, and 3D- printing. In this study comprehensive reviews of parallel robot are presented including various types of robot structure and applications which are the delta robot, 2 DOF Parallel robot, 3 DOF Parallel robot, 4 DOF Parallel robot, R4 Parallel robot, 5R Parallel robot, 6 DOF Parallel robot, Cable-driven robot, and Parallel quadruped robot. The key contributions can be summarized as follows:

- To provide a comprehensive analysis of control strategies for various types of parallel robots.
- To present a control platform for those interested in the control of parallel robots.
- To summarize the conclusions drawn from various control methods applied to different structures of parallel robots.

This paper rigorously examines the dynamics of various types of parallel robots. The study meticulously scrutinizes nine specific types of parallel robots, including the delta

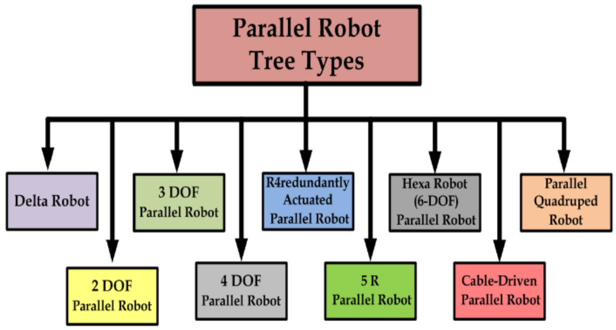

FIGURE 1. **The tree of parallel robot types.**

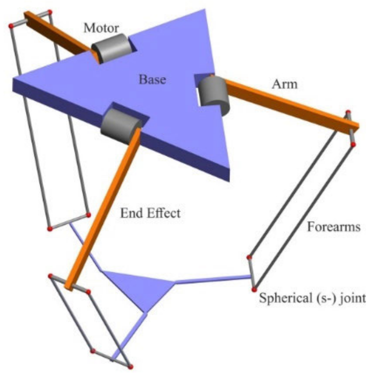

FIGURE 2. **The delta robot.**

robot, 2 DOF Parallel robot, 3 DOF Parallel robot, 4 DOF Parallel robot, R4 Parallel robot, 5R Parallel robot, 6 DOF Parallel robot, Cable-driven robot, and Parallel quadruped robot. Next, it explores the different controllers used with each type of parallel robot for multi-level analysis.

The paper has been organized as follows. In Section II, the types of parallel robots are introduced, and the dynamic and applied controllers for each one of the previously mentioned parallel robots are discussed. Section III has been devoted to the paper's conclusions.

II. TYPES OF PARALLEL ROBOT

Having explored the various types of parallel robots, including the Delta Robot, 2 DOF Parallel Robot, 3 DOF Parallel Robot, 4 DOF Parallel Robot, R4 Redundantly Parallel Robot, 5 R Parallel Robot, 6 DOF Parallel Robot (Hexa Robot), Cable-Driven Parallel Robot, and Parallel Quadruped Robot, the parallel robot tree types are shown in Figure (1). In what follows, brief descriptions of control approaches are conducted.

A. DELTA ROBOTS

Delta robot is a successfully commercialized and well-known industrial parallel robot invented by Dr. Reymond Clavel in 1985 for its ability to execute minute, precise motions. Some applications of delta robots are the packing industry, medical operations, soldering, and food processing. However, some drawbacks accompany their uses, including an incapability to carry heavy loads, limitation of the working area, low-load capacity and high prices [12].

1) DYNAMICS OF DELTA ROBOT

The diagram in Figure (2) clearly illustrates the schematic diagram of a Delta robot, which comprises two platforms: a fixed base platform and a mobile platform joined by kinematic chains. Each kinematic chain consists of the arm and the forearm [13]. The fixed base is mounted to the frame, where the passive arm is a parallelogram attached to a moving platform. The platform is maintained perpendicular to the base [14]. Rotational joints securely attach the robot arms to the actuators on the fixed platform. The robot forearms comprise two parallel bars that securely connect the arm to the mobile platform through ball joints. The end-effector is unequivocally positioned on the mobile platform [15].

To present the dynamic model of the Delta robot in joint space, the state variables are denoted as $= [q_1, q_2, q_3]^T$. Then, the dynamic model can be derived and described by the Euler–Lagrange's equations (1) as [16]:

$$\frac{d}{dt}\left(\frac{\partial L_m}{\partial q}\right) - \frac{\partial L_m}{\partial q} = Q \tag{1}$$

where q refers to the active joint angles, X_p, Y_p, Z_p the end effector position and $\phi_i (i = 1, 2, 3)$; Q refers to the applied forces to F_{pX}, F_{pY}, and F_{pZ} at point P and the applied torques $\tau_i (i = 1, 2, 3)$; to the active joints; L_m is the Lagrangian, which is obtained by the following equation as $L_m = T_m - V_m$ in which and respectively refer to the kinetic energy and the potential energy as:

$$T_m = \frac{1}{2}m_p\left(\dot{x}_p^2 + \dot{Y}_p^2 + \dot{z}_p^2\right) + \frac{1}{2}m_1 L_1^2 \sum\nolimits_i \dot{\phi}_{l_i}^2 + \frac{1}{2}m_2 \sum\nolimits_i \left(\dot{x}_p^2 + \dot{Y}_p^2 + \dot{z}_p^2 + L_1^2\dot{\phi}_{l_i}^2\right) \tag{2}$$

$$V_m = m_p g Z_p + \frac{1}{2}m_1 g L_1 \sum\nolimits_i sin\phi_{l_i} + m_2\, g \sum\nolimits_i (Z_p + L_1 sin\phi_{l_i}) \tag{3}$$

where m_p, m_1 and m_2 are the masses of the end-effector, the upper link and the lower link, respectively, L_1 represent the manipulator's length. Rearranging the terms, the inverse dynamic model of the DPR can be written into the standard joint space form as follows [15]:

$$M(q)\ddot{q} + C(q, \dot{q})\dot{q} + G(q) = \tau \tag{4}$$

where M (q) , C (q,$\dot{q}$) , and G (q) represent the inertia matrix, the matrix of Coriolis and centrifugal terms, and the vector of gravitational forces respectively, which is described by:

- $M(q) = I_{AA} + J_{inv}^T M_p \mathrm{J_{inv}}$ (5)
- $C(q, \dot{q}) = J_{inv}^T M_p J_{inv}$ (6)
- $G(q) = T_{GP} + T_{AG}$ (7)

The Delta parallel robot's dynamic equation, assuming the actuating joints frictions and the gear reducers, can be written as follows [13]:

$$\tau = A\,\ddot{q} + T_{cc}\,\dot{q} + T_g + \sum\nolimits_{i=1}^{3} \tau_{M,i} + F_v\,\dot{q} + F_c\,sgn\,(\dot{q}) \tag{8}$$

where q is the angle matrix of the driving arms, F_v is the viscous friction coefficient, and F_c is the Coulomb friction. The position of the tool center point was determined by Jacobian matrix, then the inertia matrix A can be seen, also the Coriolis/centripetal matrix T_{cc}, the matrix of gravity T_g vary with the tool center point position, and $\tau_{M,i}$ is the actuating and passive arm i.

Dynamic coupling effect between the arms can cause the kinematic chain interaction motion. Even so, the Delta parallel robot is still a time-varying coupling with a built-in uncertainty, nonlinear dynamic system, assuming no external disturbance exists [13].

2) CONTROL SCHEMES FOR DELTA ROBOT

This part will briefly discuss the most important control strategies used for motion control of the Delta robot, where designing a Delta robot's control to carry out diverse operations is demanding. These controllers are Augmented Nonlinear PD Control, Identification – Based Control, Image-Based Control, Lagrangian Formulation-Based Control, Hedge Algebras Control, B-Spline Neural Network Control, Fuzzy Logic Control, Fuzzy Logic based Neural Network Control, Adaptive Robust Control, and Robust H_∞ control, and fault tolerant controllers.

a: AUGMENTED NONLINEAR PD CONTROL

Humaidi et al. [17] designed two controllers for a Delta/ParIV-like parallel robot: an augmented PD (APD) controller and an augmented nonlinear PD (ANPD) controller.

The Augmented NPD (ANPD) Control Design for the Delta Robot was synthesized by replacing the linear PD with an APD controller structure on the based-on NPD algorithm. Figure (3) shows the Delta/ParIV-like Robot control scheme based on an augmented PD controller block diagram. The controller consists of two parts: the PD-based control law first and the feedback signal second. Furthermore, the PD-based control can be either an augmented PD controller (APD) or an augmented nonlinear PD controller (ANPD) [17].

The proposed NPD control law for Delta/ParIV-like robot,

$$\tau_d = M\,\ddot{x}^d + C\dot{x}^d + k_p\,(e)\,e + k_d\,(\dot{e})\,\dot{e} \tag{9}$$

where $\dot{x}^d$ and $\ddot{x}^d$ are the desired velocity and desired acceleration of travelling plate, respectively, and $e = [e_x e_y e_z]^T = x^d - x$ is the position error, $x = [x\ y\ z]^T$.

While in Humaidi et al. [18] incorporated the Particle Swarm Optimization (PSO) technique to optimize the controller parameters for improved dynamic performance.

This study's results showed that the ANPD controller improves tracking accuracy by 78.26% compared to APD and performance by 75% compared to NANPD [17]. The

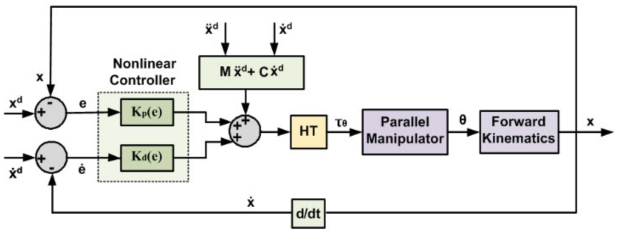

FIGURE 3. Block diagram of ANPD controller.

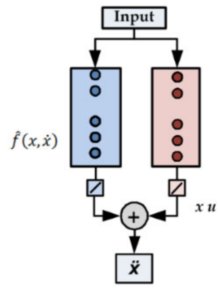

FIGURE 4. The Delta robot with the neural network model flowchart.

simulation results in [18] unequivocally demonstrate that the ANPD controller outperforms the APD controller in both tracking accuracy and robustness when evaluating controllers for trajectory tracking control using a circular path.

b: IDENTIFICATION – BASED CONTROL

Zhao et al. [19] established a control-affine neural network model for the Delta robot utilizing stepper motors. The neural networks were trained using randomly sampled data from an extensive workspace. The structure of the suggested neural network model for the Delta robot is depicted in Figure (4).

The control-affine model is relatively nonlinear straightforward, accepting joint angles and velocities from a stepper motor as shown in the following:

$$\ddot{x} = f(x,\dot{x}) + g(x,\dot{x})u \tag{10}$$

where $x = [px, py, pz]^T$, $u = [\theta_1, \theta_2, \theta_3, \dot{\theta}_1, \dot{\theta}_2, \dot{\theta}_3]^T$, $f(\cdot)$, and $g(\cdot)$ are nonlinear functions of their arguments, and p_x, p_y, and p_z represent the position of the end effector at the centroid along the x, y, and z axes.

Also, to control trajectory tracking, a sliding mode controller is designed utilizing the neural network model. The following outlines the design of the sliding mode control:

$$u\,(t) = \hat{g}^{-1}\left(\gamma\,\tanh\left(\frac{s}{\epsilon}\right) + \alpha s + C\,(\dot{x}_d - \dot{x}) + \ddot{x}_d - \hat{f}\right) \tag{11}$$

where C is positive-definite and satisfies the Hurwitz stability condition, $\gamma > 0$ and $\alpha > 0$ are constant gains, and $\epsilon > 0$. Chattering is an epidemic related concernment with sliding mode controllers with switching term sgn(s).

The neural network model, in cooperation with the sliding mode controller, obtained excellent numerical trajectory

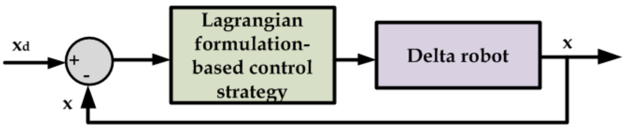

FIGURE 5. System dynamic model using an S-Function coded controller.

tracking results and performance, achieving error less than the Delta robot's average of 5 cm.

3) IMAGE-BASED CONTROL

Three types of controllers, 1) leg-direction-based visual servoing, 2) line-based visual servoing, and 3) image moment visual servoing, were designed by Zhu et al. [20]. The Delta robot is controlled via the camera image plane, which is set parallel to the end-effector. The camera frame origin is positioned explicitly at (0, 0) to ensure symmetrical observation of all robot legs [20]. According to the study, the robot designed for image moment visual servoing exhibited greater compactness and improved accuracy compared to the other two control techniques. The next phase involved conducting experimental work on actual prototypes, a crucial step to validate the simulation results. The differences in size and accuracy between the line-based controller and the image moment controller were found to be within an acceptable range, reinforcing the reliability of the simulation results.

4) LAGRANGIAN FORMULATION-BASED CONTROL

Lee et al. [21] developed an effective strategy for tracking controllers for a Delta robot based on applying the Lagrangian equations of motion for the articulated closed-chain mechanism and incorporating the Lagranign multipliers for the constraints. As shown in Figure (5), a tuned PID controller was applied to track the trajectories of movable platforms while developing a controlling strategy and considering the constraints.

The results confirmed that the Lagrangian formulation-based strategy can design effective tracking controllers for Delta robot mechanisms satisfactory tracking performance using the developed controller with Lagrangian multipliers.

a: HEDGE ALGEBRAS - BASED CONTROL

Bui et al. [14] implemented a Hedge Algebras (HA) Controller that can lead the 3 DOF delta parallel robot's direction besides the implementation of experimental models and comparative simulations for both the FLC and PID controllers.

A schematic description of the three HACs coupled to the Delta robot platform for trajectory controlling the Delta robot's three servo motors was explored and shown in Figure (6), depending on the error calculation from the actual location of the joint and the desired position difference [14].

Compared to FLC and PID controllers, the results showed that the proposed control scheme based on HAC gives better

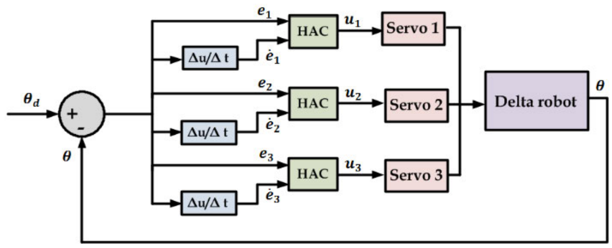

FIGURE 6. The system's control diagram in trajectory control of the delta robot.

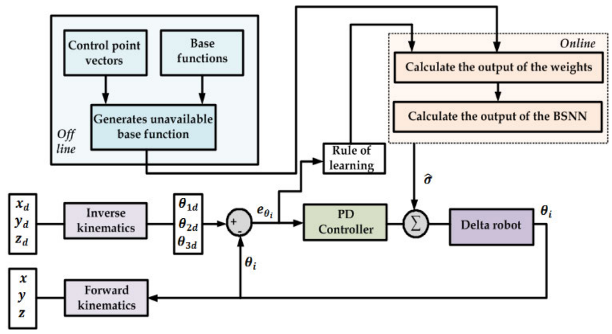

FIGURE 7. DRR control with BSNN compensation scheme.

performance and efficacy in terms of tracking error accuracy and robustness characteristics against disturbing load.

b: B-SPLINE NEURAL NETWORK CONTROL

E.-Hernández et al. [15] designed PD controller based on an artificial B-Spline neural network (BSNN) as an intelligent satisfaction of instant training to control the Delta Parallel Robot (DPR) trajectory tracking, where they used some numerical simulations under two different scenarios to calculate the controller parameters, to reach effectiveness reduce the trajectory tracking error. The BSNN is used as a feed-forward satisfaction term, which is started offline to generate the base function and depends on control point vectors to start the online part by calculating the output weights and the BSNN. Figure (7) shows the whole DPR control diagram.

An improvement of intelligent compensation was shown in the system's results under different requirements, and another controller advantage unnecessary system's dynamic parameters knowledge, taking into consideration the range of potential values for the error signal [15].

c: FUZZY LOGIC CONTROL

The Type-1 and Type-2 Fuzzy Logic controllers were designed by Lu et al. [22] for Delta robot trajectory control, where the control process of T1 FLC is described in linguistic knowledge, and it is composed of four significant parts: input fuzzification, fuzzy inference engine, fuzzy rule base and output defuzzification, where it's a system that maps crisp inputs to a crisp output. However, the optimized IT2 FLC is established by a set of simulations and comparison to its

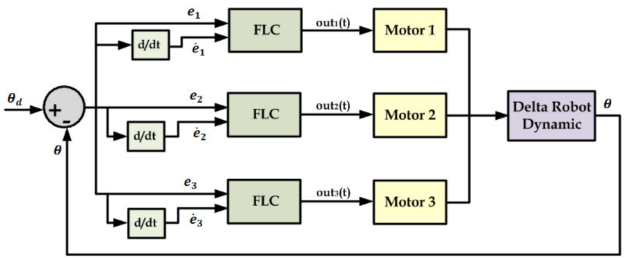

FIGURE 8. The fuzzy control system of the delta parallel robot.

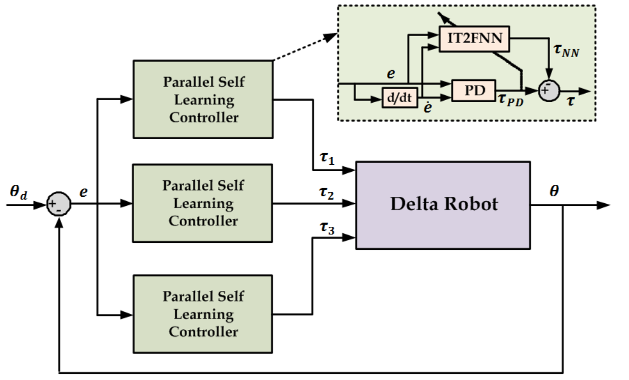

FIGURE 9. Structure of delta robot (SLIT2FNN) control scheme.

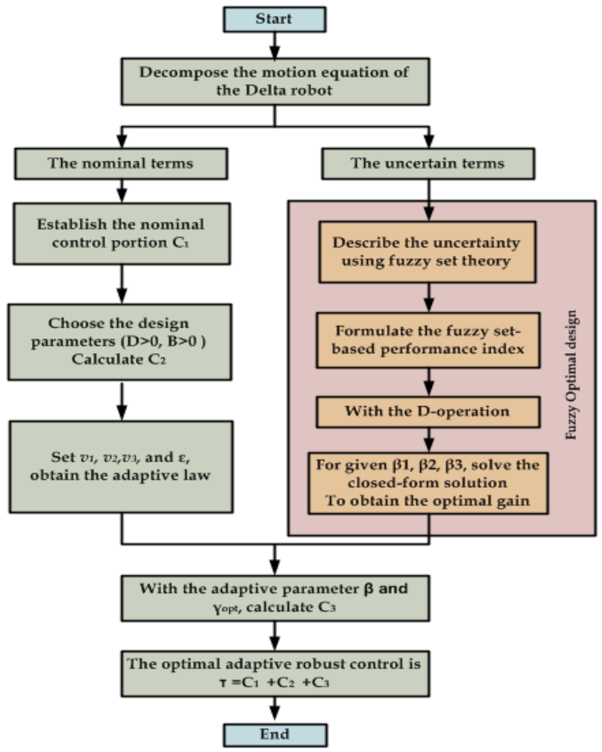

FIGURE 10. The optimal design procedure flow chart.

type-1 counterpart even if external and internal uncertainties exist, the proposed controllers shown in figure (8) [22].

This study illustrated that the optimized IT2 FLC is proved via a set of simulations and Type-1 results comparison counterpart even if external and internal uncertainties exist. The results showed that the optimized IT2 FLC can support more accurate trajectory tracking performance.

d: FUZZY LOGIC BASED NEURAL NETWORK CONTROL

The Interval Type-2 Fuzzy Neural Network (IT2FNN) controller was designed by Lu et al. [13] to control a Delta robot trajectory. This controller has a parallel structure that combines an (IT2FNN) controller and a traditional Proportional-Derivative (PD) controller, where Type-2 fuzzy membership functions (IT2MF) were suggested as a trapezoidal interval arrangement, which has an analytical form of the adaptation laws. They presented a learning algorithm based on sliding mode control (SMC) theory for training the IT2FNN system parameters [13].

Adjustments have been made to the primordial IT2FNN-0 architecture, and the construction is shown in Figure (9). There are two kinds of network nodes: fixed nodes and adaptive nodes. The first node has a modifiable parameter illustrated by squares, while the second node illustrates by circles that can be settled performed with math operations [13].

The suggested controller illustrates the difficulty of trajectory tracking the Delta robots in the uncertain appearance of constructed and unconstructed. The results showed that the suggested SLIT2FNN controller technique produces higher performance with trajectory tracking accuracy and is more robust to uncertainties than its equivalent [13].

e: ADAPTIVE ROBUST CONTROL

Wu et al. [23] used an Adaptive Robust Controller to ensure the delta robot was uncertain despite minimizing a performance index based on fuzzy sets. An adaptation mechanism of the optimized robust controller consisting of the leakage term and the dead zone to estimate the uncertainty data, different from the conventional if-then rules-based fuzzy control, can guarantee the system performance in two aspects: the uniform boundedness and uniform ultimate boundedness, which is the deterministic performance and related with the specific demands of the robot (such as the control precision); the fuzzy performance associated with the optimization of the robust control gain in the sense of the fuzzy dynamic systems. The suggested controller scheme is deterministic and fuzzily optimized [23].

Compared to traditional robust controller techniques, the suggested optimal robust control is more practical and cost-effective for the Delta robot. Motivated by fuzzy optimal controller design, exploring further applications in other system's dynamics is interesting. The optimal design strategy can be seen in Figure (10)

A series of simulation experiments illustrate the effectiveness of the used controller, where the suggested controller scheme is deterministic and fuzzily optimized. The experiments conclusively establish that a unique global

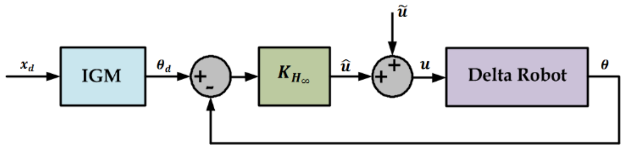

FIGURE 11. The H_∞ control scheme with delta robot.

solution in closed form exists for this optimal design without exception.

f: ROBUST H_∞ CONTROL

Rachedi et al. [24] designed an H_∞ multi-variable controller for a delta robot using a mixed sensitivity approach in which the sensitivity function matrix S and the complementary sensitivity function matrix T are considered. Also, they compared the centralized H_∞ controller with a classical decentralized Proportional Integral Derivative (PID) controller. Linearization of the dynamic model of the Delta robot Determination is a prerequisite to control the Delta robot using the H_∞ controller. The schematic diagram of the H_∞ control is shown in Figure (11).

The synthesized controller $K_{H\infty}$ was implemented in the centralized control scheme represented by Figure (3), X_d represents the desired trajectory coordinates in the tool space. The inverse geometric model (IGM) gives the corresponding desired joint coordinates. In this study, the steady-state root mean square error of the $H\infty$ was improved to 60% compared to the results of the PID controller [24].

g: FAULT TOLERANT CONTROL

Mazare et al. [25] proposed a new method for delta parallel robots called fault-tolerant control (FTC). This method combines adaptive high-order super-twisting (AST) control with nonsingular integral-type terminal sliding mode (NITSM) control, collectively referred to as AST-NITSM. Additionally, they employ the Harmony Search Algorithm (HSA) to fine-tune the controller parameters to optimize system performance. The optimization is guided by two goals: minimizing the control signal rate and reducing the integral time absolute error (ITAE).

Where the proposed control equation as in the following:

$$\begin{aligned}
\tau_{AST-NITSM} &= M(q)\ddot{q}_d + C(q,\dot{q})\dot{q} + G(q) \\
&\quad - M(q)\left[2\lambda\dot{e} + \lambda^2 e + A\alpha|e|^{\alpha-1}\dot{e} + \kappa\frac{b}{c}\dot{e}e^{\frac{b-c}{c}}\right] \\
&\quad - \left(\xi\sqrt{\|S\|}sgn(S) + \int \eta sgn(S)\,dt\right) \qquad (12)
\end{aligned}$$

where κ is a positive constant, c and b are positive odd numbers which $b < c$

According to their results, the AST-NITSM controller outperforms traditional sliding mode and feedback linearization control methods, particularly when faced with uncertainties, unknown external load disturbances, and actuator faults.

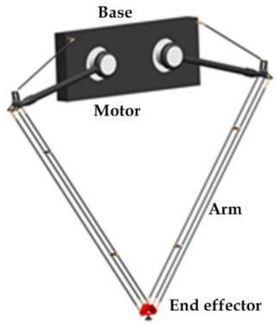

FIGURE 12. The 2 DOF parallel robot.

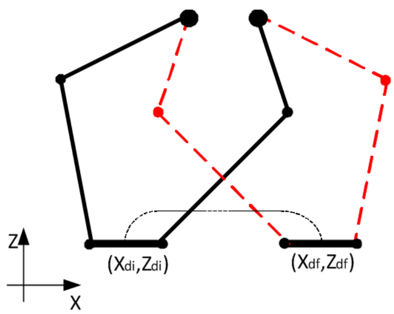

FIGURE 13. Illustration of the robot's movements.

B. 2-DOF PARALLEL MANIPULATOR

Most parallel mechanisms with 2-DOF are planar manipulators with two translational degrees of freedom (DOFs), which may use both prismatic and revolute joints in the design. The robot consists of a movable platform, two uniform kinematic chains, and a base. The robot supports the movable platform in an ability with a 2-DOF translational motion independently driven by two active proximal links, the first one has a fixed direction mechanism of robot rotation motion properties, while the second has variable directions of both the rotation and the translation motion properties, as shown in Figure (12) [26].

Examples of its applications are machining and assembling. The limitation of enhancing the pose accuracy of the moving platform and making the life service of the manipulator shorter because of some geometric errors result in internal forces and deformations.

The ParII parallel manipulator for one cycle of a pick-and-place trajectory, that is, the robot's platform has to go from the preferred 'pick' Cartesian position (x_{di}; z_{di}) to the preferred 'place' Cartesian position (x_{df}; z_{df}) and then return to the initial one (x_{di}; z_{di}). The conformable Cartesian desired trajectory and the representation of the robot's motions are illustrated in Figure (13) [27].

1) DYNAMICS OF 2 DOF PARALLEL ROBOT

In this paper, the Lagrangian nonlinear dynamic model matrix form of robot manipulators that can make use of the control and monitoring tools as described in the following equation [26], [27]:

$$I(q)\ddot{q}+C(q,\dot{q})\dot{q}+G(q)+f(q,\dot{q})=\tau \tag{13}$$

where $q^T = [q_1, q_2, \ldots, q_n] \in \mathbb{R}^n$ represent the vector of positions, $\dot{q}^T = [\dot{q}_1, \dot{q}_2, \ldots, \dot{q}_n] \in \mathbb{R}^n$ represent the vector of velocities, $\ddot{q}^T = [\dot{q}_1, \dot{q}_2, \ldots, \dot{q}_n] \in \mathbb{R}^n$ represent the vector of accelerations, $I(q) \in \mathbb{R}^n$ represent the inertia matrix, $C(q,\dot{q}) \in \mathbb{R}^n$ represent the matrix of Coriolis and centrifugal terms, $G(q) \in \mathbb{R}^n$ represent the vector of gravitational forces, $f(q,\dot{q}) \in \mathbb{R}^n$ represent the vector of friction forces, $\tau \in \mathbb{R}^n$ represent the vector of control inputs refers to the torques developed by the actuators [26], [27].

2) CONTROL SCHEMES FOR 2 DOF PARALLEL ROBOT

This part will briefly discuss the most important control strategies for 2 DOF parallel robot motion control. These controllers are Observers – Based Control, Sliding Mode – Based on Backstepping Control, Nonlinear Dual Mode Adaptive Control, and Robust Adaptive Control.

a: OBSERVERS - BASED CONTROL

The purpose of this research is to implement state Observers controllers for parallel manipulators (ParII) by Natal et al. citebib:27. These controllers include a Lead-lag filter-based observer, an Alpha-beta-gamma observer and a High-gain observer. A key part of this study is to compare the performance obtained of the trajectory tracking with a maximum acceleration of 15G to those reached by applying a nonlinear Dual Mode (DM) controller [26].

This control law of DM controller was given by equation:

$$\tau = Y\hat{a}+K.s+\bar{d}\mathrm{Sat}(\alpha s) \tag{14}$$

where $s = \dot{q}+\lambda\check{q}$, being $\check{q} = q_d - q, \dot{q} = \dot{q}_d - \dot{q}(q,\dot{q}$ and $\ddot{q})$ are the vectors of positions, velocities and accelerations and (q_d, $\dot{q_d}$ and $\ddot{q_d}$) are their desired trajectories, respectively); $\lambda, \bar{d}, \alpha$, and K are positive coefficients, $\mathrm{Sat}(\alpha s) = \frac{\alpha s}{\|\alpha s\|+1}$ is a smooth and continuous saturation function concerning its reasoning (with continuous partial derivatives and restricted constituent to the interval $[-1; +1]$). The vector $\hat{a}$ shows an unknown parameters approximation of the system named by the vector the vector a, and $Y(q,\dot{q},\ddot{q})$ is the regressor vector, which is based on the dynamic model of the system [27].

The performances achieved in real-time experiments by each observer have been thoroughly documented and compared. It was possible to observe that the DM controller has the possibility of a good tracking performance in all cases as a result of the good velocity estimation [27].

b: SLIDING MODE- BASED ON BACKSTEPPING CONTROL

In Mostafa et al. [28] applied a nonlinear backstepping sliding mode design scheme and then developed a switching function for high-accuracy tracking of a mixed space trajectory for the motion control of a 2-degree-of-freedom (2DoF) planar parallel robot. The dynamic equations of motion are considered structured and unstructured uncertainties. The simulation

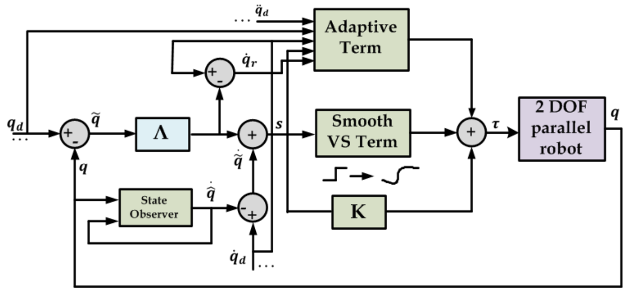

FIGURE 14. The dual mode control scheme block diagram.

results demonstrated that the backstepping sliding mode controller for the 2DoF parallel robot with a Biglide type and elastic joints outperformed the PID controller, sliding mode controller (SMC), and Computed Torque Control (CTC) in terms of robustness and trajectory following performance.

c: NONLINEAR DUAL MODE ADAPTIVE CONTROL

A nonlinear dual mode adaptive controller was applied by Chemori et al. [26], for both non-redundant PAR2 parallel manipulators for 2D pick-and place trajectories and redundantly actuated parallel manipulators pick-and-place trajectories. Also G. Natal et al. [29], they implement a linear Proportional-Derivative (PD) controller and a nonlinear/adaptive Dual Mode (DM) controller (complied with the High-gain observer for joint velocity estimation) for ParII parallel manipulator for pick-and-place applications.

A nonlinear dual-mode controller is derived from the nonlinear adaptive controller in addition to the dropping on the law of parametric adaptation. It reduces the effective gain of the controller when the tracking error increases [25]. This control law is given by:

$$\tau = Y\,\hat{a}+K.s+\bar{d}\,\mathrm{Sat}(\alpha s) \tag{15}$$

where $s = \dot{q}+\lambda\check{q}$, being $\check{q} = q_d - q$, $\dot{q} = \dot{q}_d - \dot{q}(q,\dot{q}$ and $\ddot{q})$ are the vectors of positions, velocities and accelerations and (q_d, $\dot{q_d}$ and $\ddot{q_d}$) are their desired trajectories, respectively); $\lambda, \bar{d}, \alpha$ and K are positive constants, $\mathrm{Sat}(\alpha s) = \frac{\alpha s}{\|\alpha s\|+1}$ is a smooth and continuous saturation function with respect to its argument (with continuous partial derivatives and components limited to the interval $[-1; +1]$). The vector $\hat{a}$ represents an estimate of the unknown parameters of the system given by the vector a, and $Y(q,\dot{q},\ddot{q})$ is the regressor vector (based on the dynamic model of the system) [26], [29].

The control architecture of the dual-mode adaptive controller is illustrated in Figure (14).

A dual-space adaptive controller is an advanced iteration of the dual-space feed-forward controller depicted in Figure (15), designed to enhance the controller's robustness significantly. The dual-space feed-forward controller is a concept that involves using a PID controller in Cartesian space and employing the pseudo-inverse matrix to address actuation redundancy. Additionally, two feed-forwards in joint

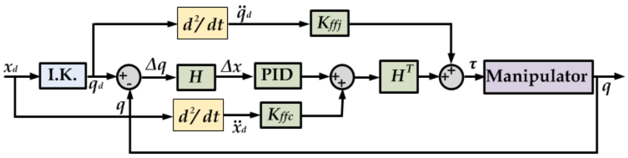

FIGURE 15. The dual-space feedforward controller.

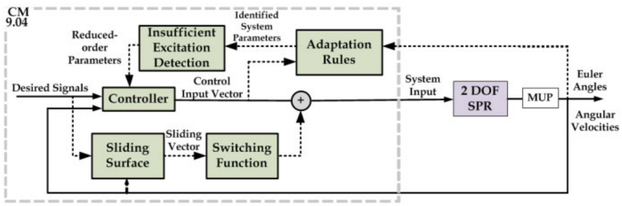

FIGURE 16. The identification procedure.

and Cartesian spaces enhance the controller's tracking performance.

The results reached by Chemori et al. showed the controller effectiveness, which was demonstrated through the experimental results obtained after implementing the two prototypes in real-time [26]. Those reached by Natal et al. showed that the DM controller has a significantly better performance than the PD controller, and in this case study, an Alpha-beta-gamma (ABG) observer has the ability to generate the best estimation of the joint's velocity. Also, an important issue for higher accelerations was noticed from small mechanical vibrations after reaching 20G of acceleration [29].

d: ROBUST ADAPTIVE CONTROL

The Robust Adaptive Scheme considers the presence of bounded disturbances for the identified transfer function of a 2DOF parallel robot. Rad et al. [30] introduced the suggested modern, robust adaptive structure and the solution for insufficient excitation based on the order-decrease models. A system's simultaneous identification and control of exterior disturbances was implemented on a 2-degree-of-freedom spherical parallel robot as a stabilizer device with model uncertainties and disturbances.

The identification procedure is initiated by measuring data from the gyrator sensor, which includes Euler and angular velocities. This data is then transmitted to the controller, where the Robust Adaptive Scheme is employed. The controller uses this scheme to measure the data and adapt the control input, updating the identified system parameters.

The relationship between different components of the identification process is illustrated in Figure (16).

The result shows dependable performance in tracking selected paths for the end-effector Euler angles [30]. These results were obtained after the Jacobian matrix identified unknown parameters. The comparative identification error is obtained as 0.0207 [30].

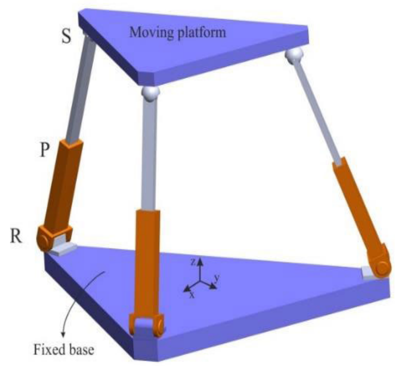

FIGURE 17. The 3 DOF parallel robot.

C. 3 DOF PARALLEL ROBOT

Parallel manipulators have an inflexible structure and can pick up objectives with heavy weights. The three revolute joints are used to achieve the mechanism operation of the parallel planar robot [31]. These types of robots can effectively avoid singularities at the zenith angle while tracking due to their unique kinematic characteristics [32].

A crucial group of parallel mechanisms has garnered significant attention. They all share a defining characteristic: the mobile platform possesses complex degrees of freedom, including three independent degrees of freedom (one translation and two rotations) [2]. The rotational joints (R-joints) are attached to the base, and the spherical joints (S-joints) are attached to the moving platform. The leg lengths are adjustable by prismatic joints (P-joints). Where rotational joints (R-joints) are attached to the base and the spherical joints (S-joints) are attached to the moving platform. The leg lengths are adjustable by prismatic joints (P-joints) [2].

Therefore, a parallel manipulator has been developed based on the cooperation of three arms of a robotic system to make the whole system suitable for solving many problems such as [2]: flight simulator, polishing machine, earthquake wave simulator, high cost, small workspace, complex forward kinematics, complicated forms, materials handling, and industrial automation.

The kinematics of the 3DOF parallel robot contain three leading chains: a serial of an arm; the forearm, which is composed of two parallel bars; the travelling plate, the motors are used to change the angles of the parallel manipulator arms provide three degrees of freedom rotational motion that produce changing the location and orientation of the travelling plate. Because of this structure, the robot has the ability to move the mobile plate with three translation movements, as shown in Figure (17) [33].

1) DYNAMICS OF 3-DOF PARALLEL ROBOT

The dynamic model of the 3-RRR parallel manipulator can be developed based on the dynamic model of the serial manipulator. Determining the constant coefficients for each serial

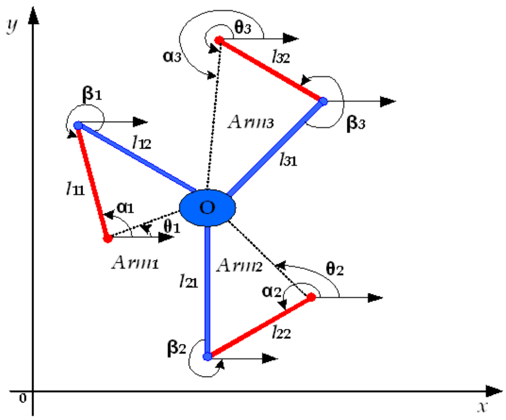

FIGURE 18. The structure of 3-RRR planar parallel robotic platform.

kinematic chain of a parallel robot is essential.

$$\alpha_i = J_{ai} + m_{ai}\, r_{ai}^2 + m_{bi} l^2 \tag{16}$$

$$\beta_i = J_{bi} + m_{bi}\, r_{bi}^2 \tag{17}$$

$$\gamma_i = m_{bi}\, l\, r_{bi} \tag{18}$$

where $i = 1, 2, 3$, m_{ai} and m_{bi} refer to the links masses, J_{ai} and J_{bi} denote the links moments of inertia, that is directly associated with the distances between mass centers and joints of the links, represented as r_{ai} and r_{bi}, as well as the length of the links, denoted as l. Utilizing the provided equation, we definitively establish the dynamics of serial kinematic chains. When we combine the dynamics of the 3 serial chains and factor in the constraint forces stemming from the closed-loop constraints, we assertively formulate the dynamic model of the parallel manipulator in the joint space as follows:

$$M\,\ddot{\theta} + C\,\dot{\theta} = \tau \tag{19}$$

where $\theta = [\theta_{a1}, \theta_{a2}, \theta_{a3}, \theta_{b1}, \theta_{b2}, \theta_{b3}]^T$ defines the vector of joint positions, $\tau = [\tau_{a1}, \tau_{a2}, \tau_{a3}, \tau_{b1}, \tau_{b2}, \tau_{b3}]^T$ denotes the vector of input [34], [35].

Kinematics Model for 3-RRR Parallel Robot [31].

The kinematics model for the 3-RRR parallel planar robot is classified into two models: the forward kinematic model and the inverse kinematic model.

This model is used to detect the coordinate of the mobile end-effector (MEE) $a(E_x, E_y, \sigma)$ depending on values of kinematic parameters (length of active links l_{1i}, length of passive links l_{2i}, angles active links αi, the coordinate of active points (A_{ix}, A_{iy}) and the coordinate of passive points (B_{ix}, B_{iy}). From Figure (18), the following independent equations can be derived to describe the workspace of the MEE of the 3RRR parallel planar robot as shown below:

$$\begin{cases} l_{21}^2 = \sqrt{(E_x - B_{1x})^2 - (E_y - B_{1y})^2} = D(B_1, E) \\ l_{21}^2 = \sqrt{(E_x - B_{2x})^2 - (E_y - B_{2y})^2} = D(B_2, E) \\ l_{23}^2 = \sqrt{(E_x - B_{3x})^2 - (E_y - B_{3y})^2} = D(B_3, E) \end{cases} \tag{20}$$

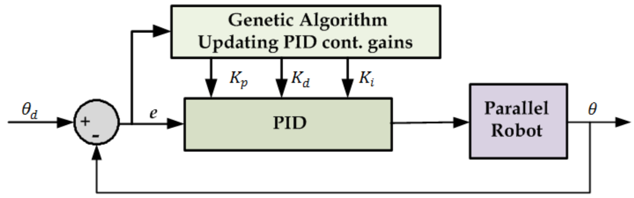

FIGURE 19. System proportion integration differentiation (PID) closed-loop control block diagram.

D. CONTROL SCHEMES FOR 3 DOF PARALLEL ROBOT

This part will briefly discuss the important control strategies utilized for motion control of the 3 DOF Parallel Robot. Designing the control for a 3 DOF Parallel robot to execute different operations is challenging. These controllers are PID Control, Genetic Algorithm Optimized PID Control, Model-Based control, Cooperative Control, Fuzzy PID Control, Fuzzy- Based PID Control, Interval Type-2 Fuzzy Logic Control, and fault tolerant Controller.

1) PID CONTROL

A PID-type controller was designed for 3 DOF parallel robots that use revolute and spherical joints by Ruiz-Hidalgo et al. [36]; they also presented the inverse kinematic model. PID controller designed for position reference tracking and robust tracking to the desired position trajectory for the movable platform position; consider the equation below :

$$F_i = m_i\left(\ddot{z}_{id} - K_d(\dot{z}_i - \dot{z}_{id}) - K_p(\dot{z}_i - \dot{z}_{id}) - K_{id}\int(\dot{z}_i - \dot{z}_{id})\,dt\right) + b_i z_i \tag{21}$$

where K_p is the proportional action, K_{id} is the integral action, K_d is the derivative action, and $(\dot{z}_i - \dot{z}_{id})$ is the angular position error e. Given by the real position z_i measured from simulation minus a desired position z_{id} given by the desired path [36].

The results were a virtual prototype simulated under the Automatic Dynamic Analysis of Mechanical Systems (ADAMS) environment, which showed the effectiveness of the proposed controller [36].

2) GENETIC ALGORITHM OPTIMIZED PID CONTROL

Sheng et al. optimized the PID controller parameters using a genetic algorithm controller for the inverse kinematics model of the 3-Revolute–Revolute–Revolute (3)-RRR) parallel robot, the PID controller closed-loop system block diagram is shown in Figure (19) [34].

The results showed better control precision, stability and robustness as compared with that of classical PID controller [34].

3) MODEL-BASED CONTROL

D.-Rodríguez et al. [33] implemented a reduced model based on a set of relevant parameters on a virtual and an actual prototype for the 3-DOF prismatics-revolute-spherical parallel

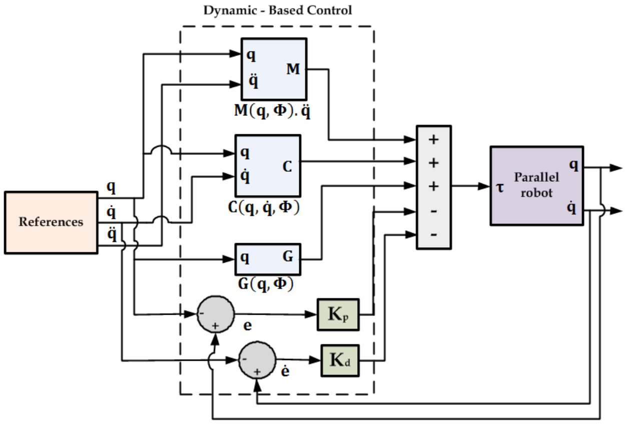

FIGURE 20. Dynamic-based control scheme.

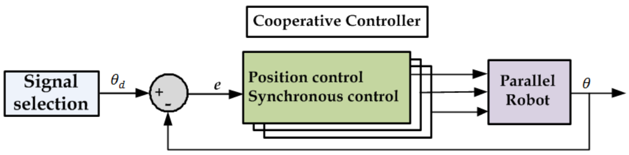

FIGURE 21. The black dashes contain the details of the whole control system framework.

manipulator. Figure (20) shows a block diagram of the control strategy.

The results indicate that the control scheme, based on the reduced model, enhances trajectory tracking precision compared to the control scheme using the complete set of dynamic parameters. Additionally, the reduced model substantially decreases the computational workload, enabling real-time control [33].

4) COOPERATIVE CONTROL

The parallel mechanism (PM) with 3 DOF has been proposed to utilize a new combined control strategy by Huang et al. [31] to achieve synchronized and differential motion. Validation of the effectiveness of the combined controller was conducted using a pneumatic actuated test rig, as shown in Figure (21).

The results indicated the proposed controller demonstrated improved tracking accuracy, smaller constitute errors, and a faster settling time compared to the PID controller. Specifically, the asynchronous movement between every two cylinders could reach up to 10 mm for the PID controller, while our cooperative controller reduced these fluctuations by almost half. Our controller unequivocally displayed a minor average difference between every two cylinders and consistently delivered a stable and reliable performance when approaching targets [31].

5) FUZZY PID CONTROL

A Fuzzy controller companied with a classical PID controller was designed to reach the optimal performance of a novel three-degrees-of-freedom (3)-DOF) parallel robot with the permanent-magnet synchronous motor (PMSM) by Li et al. [37]. The PMSM servo system using a fuzzy PID controller is shown in Figure (22) [37].

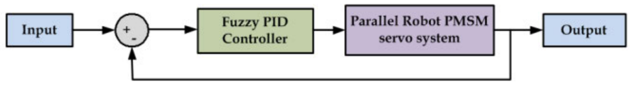

FIGURE 22. PMSM servo system using fuzzy PID controller.

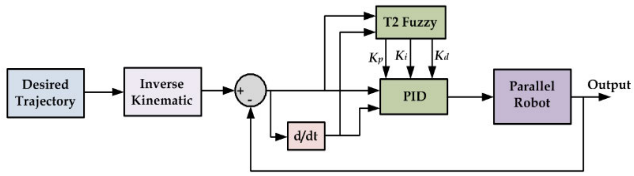

FIGURE 23. The T2 Fuzzy- PID controller scheme.

The simulation results indicate that the fuzzy PID controller offers fast response, minimal overshoot, reduced regulation time, and anti-interference capabilities [37].

6) FUZZY- BASED PID CONTROL

A new Type-II Fuzzy-PID was proposed for a 3-PRS parallel robot by Tavoosi et al. [32]. A comparison of the performance of the Type-I and Type-II Fuzzy systems indicates the superiority of the Type-II Fuzzy system. The simulation results proved that applying the Type-II Fuzzy for tuned PID controller gains shows better performance than that with applying Type-I Fuzzy systems [32], as shown in Figure (23).

7) INTERVAL TYPE-2 FUZZY LOGIC CONTROL

Najem [35] and Humaidi et al. [38] applied the following controllers: Type-1 Fuzzy Logic (T1FL) Controller and Interval Type-2 Fuzzy Logic (IT2FL) Controller to control the position of trajectory tracking and robustness characteristics for a 3-RRR parallel robot. She used Social Spider Optimization (SSO) to tune the design parameters of fuzzy logic control structures. Figure (24) shows the optimal IT2FLC (T1FLC) of a 3-RRR parallel robot based on the SSO algorithm.

The results show an improvement of 70 % with the optimized IT2FL controller, which greatly improves position tracking for different desired trajectories such as: circle, square, triangle, and infinity, as well as in a disturbance-free situation, compared to those results with the T1FL controller [35].

Humaidi et al. [38] tested two scenarios to evaluate proposed controllers' tracking performance and robustness. The scenarios were based on two square desired trajectories, one with disturbance and one without. When there was no external disturbance, the IT2FL controller outperformed the T1FL controller in both joint and Cartesian spaces. Additionally, the IT2FL controller required smaller torque for control than the T1FL controller. In the presence of external disturbances,

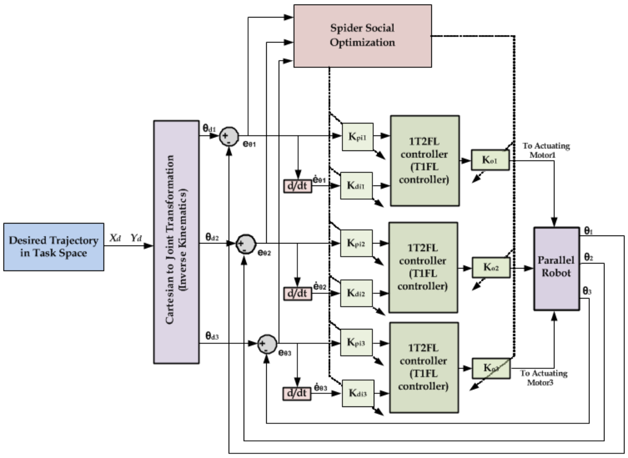

FIGURE 24. 3-RRR Parallel Robot controlling with SSO-based IT2FLC (T1FLC).

simulations showed that the IT2FL controller achieved better tracking performance regarding RMSE than the T1FL controller. Furthermore, the IT2FL controller exhibited lower control effort and demonstrated more robust characteristics than the T1FL controller. This study can be implemented in real-time to verify the effectiveness of the proposed controller experimentally.

E. 4-DOFS PARALLEL KINEMATIC MANIPULATOR

Parallel manipulators offer high stiffness and low inertia, unlike serial mechanisms. In many industrial settings, equipment that offers more than 3 degrees of freedom (DOFs) is required. For instance, in semiconductor manufacturing pick-and-place applications, a minimum of 4 DOFs is necessary: 3 for translation to move the carried object from one point to another and 1 for rotation to adjust its orientation in the final location [39].

A fully actuated 4 DOF parallel manipulator, known as a parallel robot, features four identical kinematic chains. The schematic diagram of the robot is depicted in Figure (25). Each kinematic chain comprises an actuator, an arm (including the rotor part of the actuator), and a forearm fixed to the moving platform using spherical joints. The articulated moving platform can execute three translations along the x, y, and z axes and a single rotation about the z-axis. The moving platform is firmly connected to the fixed base through kinematic chains, enabling it to execute three spatial translations and one rotation around the vertical axis. The rotation is precisely achieved via the relative motion of the upper and lower parts of the moving platform. All four actuators accountable for the motion of the mechanical structure unequivocally lie on the same plane [40].

1) DYNAMICS OF 4 DOF PARALLEL ROBOT

The actuated joint coordinates are represented via vector $q = [q_1; q_2; q_3; q_4]^T$ and ultimately represent the structure of the whole mechanism.

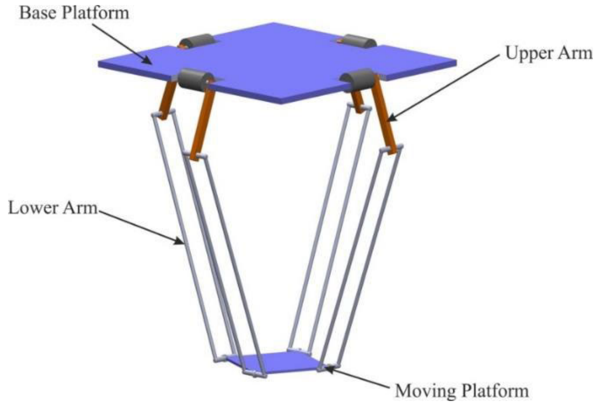

FIGURE 25. Four-DOF parallel robot schematic diagram.

The dynamic model of VELOCE can be described in a traditional joint-space form as follows [40], [41]:

$$M(q)\,\ddot{q} + C(q,\dot{q})\,\dot{q} + G(q) + \tau_f = \Gamma \tag{22}$$

where:

$M(q) = I_{tot} + (J_m^T)^{-1} M_{tot} J_m^{-1} \in R^{4\times4}$ represent the total inertia matrix.

$C(q,\dot{q}) = -(J_m^T)^{-1} M_{tot} J_m^{-1} J_m J_m^{-1} \in R^{4\times4}$ represent the centrifugal and Coriolis forces matrix

$G(q) \in R^4 = \Gamma_{flood}$ represent the vector of gravitational forces.

τ_f: represent the friction vector.

$(q, \dot{q}, \ddot{q})$: represent the position, velocity, and acceleration vectors of the joint angles

Γ: represent the torque vector generated by the actuators, defined by $\Gamma \in R^4$. [40], [41], [42], [43], [44]

Actuator faults

In the 4-DOF parallel manipulator against uncertainties such as modelling error and actuator faults. The form of the actuator, faults including lost efficiency and bias faults in the four actuators, are exhibited as follows:

$$\tau = \alpha u + \check{u} \in R^{4\times1} \tag{23}$$

where $\tau \in R^{4\times1}$ is the control signal, $u = [u1, \ldots, u4]^T \in R^{4\times1}$ displays the control input of the controllers, $\alpha = \mathrm{diag}([\alpha1, \ldots, \alpha4]T) \in R^{4\times1}$ is the arbitrary positive diagonal matrix, $\check{u} \in R^{4\times1}$ is the uncertain fault vector [44].

The subsystem addresses the challenge of tracking the 4-DOF parallel manipulator, dealing with modelling errors, unknown payload, and actuator faults.

2) CONTROL SCHEMES FOR 4 DOF PARALLEL ROBOT

This part will briefly discuss the most important control strategies used for motion control of the 4 DOF Parallel Robot, where designing the control for a 4 DOF parallel robot to carry out different operations is challenging. These controllers are Model-Based PD Control, Synchronous PD Control Based on a Time-Delay Estimator, Nonlinear Model Predictive Control, Synchronous Sliding Mode

Control, fault-tolerant synchronous sliding mode, Adaptive Control, L_1 Adaptive Control, and Adaptive Terminal Sliding Mode Control.

a: MODEL-BASED PD CONTROL

Escarabajal et al. [44] designed a model-based controller for a 4-DOF parallel robot for knee rehabilitation after applying identification techniques to estimate all dynamic parameters and a comparison between the model-based controller and PD controller with gravity benefit, where the proposed controller has been experimentally validated, it has successfully maintained stable error levels despite significant changes in the leg's weight of the patient. However, the adaptation law is used along with an underlying PD controller and can be expressed as follows [44]:

$$\vec{\tau}_c = Y(\vec{q}) \cdot \vec{\hat{\theta}}(t) + \vec{G}_{NE}(\vec{q}) - K_d \dot{\vec{q}}_{ind} - K_p \vec{e} \tag{24}$$

$$\frac{d\vec{\hat{\theta}}(t)}{dt} = -\Gamma_0 \cdot Y^T(\vec{q}) \cdot \vec{s}_1 \tag{25}$$

$$\vec{s}_1 = \dot{\vec{e}} + \lambda_1 \cdot I \cdot \vec{e} \tag{26}$$

with Y:Regressor matrix plays a pivotal role in the approximation of $\vec{\theta}_E$. This matrix, indirectly doubled by R^{*T}, is considered as $Y = K_E$, underscoring its significance in the process.

$\vec{G}_{NE}$: Non-adaptive gravitational term, also including the influence of R^{*T}, and it compensates for the unidentified, identified as relevant parameters:

$$\vec{G}_{NE} = K_{NE} \cdot \vec{\theta}_{NE}$$

K_p, K_d : Proportional and derivative gains of the PD controller.

Γ_0 and λ_1: Matrix and a scalar, which define the dynamics of the estimation process, acting like observer parameters.

They used an Online Identifier with a Window-Based Least Squares (WLS) method, which estimates the relevant parameters using least squares. The PD controller compensates for gravity using two terms: an adaptive term represented by the regressor matrix Y and a fixed term defined by the vector $\vec{G}_{NE}$. These terms are calculated similarly.

Figure (26) depicts the controller's representation applying the WLS estimator method. The vector $\vec{G}E = KE \cdot \vec{\theta}k$ represents the final gravitational effect, which is determined by the estimated relevant parameters in the equations (24, 25, and 26).

This new controller seamlessly combines identification and control, making adjusting easy. Its parameters can be easily understood, which sets it apart from traditional adaptive controllers. An experimental comparison of the performance of a conventional adaptive controller and the proposed method yields compelling insights [44].

b: SYNCHRONOUS PD CONTROL BASED ON A TIME-DELAY ESTIMATOR

Tran et al. [42] developed a controller for a parallel robot (4-DOF) by combining a synchronous proportional derivative

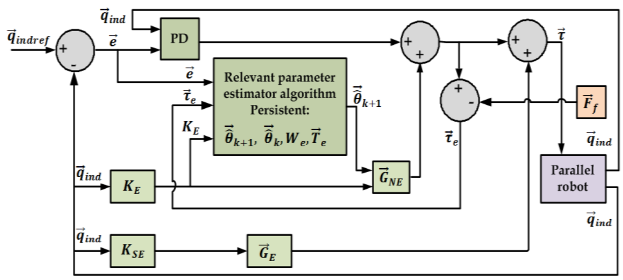

FIGURE 26. The identification of relevant parameters online using a window-based controller scheme.

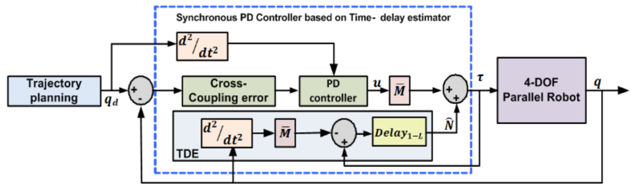

FIGURE 27. The structure of the proposed control.

(PD) control method with a time delay estimator (SPD-TDE). They aimed to estimate and eliminate uncertainty components, such as modelling errors and actuator faults, and ensure the robot's tracking objectives and synchronous requirements. They also used the Lyapunov theory to demonstrate the stability and robustness of the proposed controller. The diagram in Figure (27) presents the proposed control for a 4-DOF parallel robot in practice.

The control ensures the system output response q follows the reference trajectory q_d, so the tracking error $e = q_d - q$ congregates to zero. The desired error dynamics are defined as follows:

$$\ddot{e} + K_D * \dot{e} + K_P * e = 0 \tag{27}$$

As established in Figure (32), it is evident that the control input takes the following form:

$$\tau = \bar{M}u + \hat{N}(q, \dot{q}, \ddot{q}) \tag{28}$$

with

$$u = \ddot{q}_d + K_D * \dot{E} + K_P * E \tag{29}$$

where $\hat{N}(q, \dot{q}, \ddot{q})$ denotes the estimate of $\hat{N}(q, \dot{q}, \ddot{q})$ obtained via the TDE subsystem.

The results showed the sustainability and effectiveness of the controlled 4 DOF parallel robot response with SPD-TDE controller as compared to those after using the PD control and SPD control [42].

c: NONLINEAR MODEL PREDICTIVE CONTROL

In 2019, Kouki et al. [45] successfully utilized fast nonlinear model predictive control (NMPC) to control the parallel kinematic manipulator VELOCE. They developed a new extension of NMPC to precisely handle the system's rapid

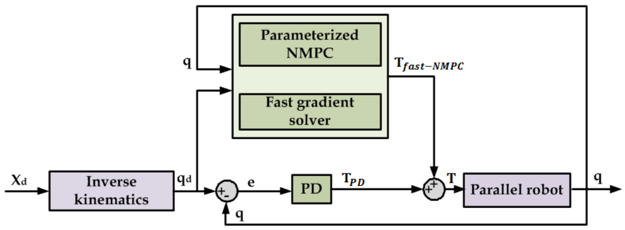

FIGURE 28. Block diagram of the proposed control scheme.

response using a parameterization technique. The primary objective was to achieve real-time control and significantly reduce computation time by decreasing the size of the optimization problem.

The conclusion control arrangement "u" can be illustrated by a low-dimensional vector "p" instead of a future control sequence. The optimal parameter vector "$\hat{p}$" is obtained by minimizing a cost function J, as described in the following [45]:

$$\hat{p} = \arg\min_{P} [J(p, X(k))] \tag{30}$$

where X(k) is the recent value of the state at time k and J(:) is the cost function to minimize

The developed control scheme incorporates a parametric process, a fast gradient solver, and an additional PD control term to significantly enhance tracking performance, as depicted in Figure (28). The proposed control law is then effectively employed to control the manipulator [45]:

$$\Gamma = \Gamma_{fastNMPC} + \Gamma_{PD} \tag{31}$$

where $\Gamma_{fastNMPC}$ is the fast NMPC control signal, while Γ_{PD} represent the control vector of the proportional derivative controller [46].

The suggested controller unequivocally showcases robust computational capabilities and consistently achieves superior control performance. Its computation time surpasses that of classical NMPC, thereby ensuring the resolute robustness of the resulting closed-loop system [45].

d: SYNCHRONOUS SLIDING MODE CONTROL

Tran et al. [41], after applying the following controllers: classical PID, synchronous control algorithm with a conventional PID controller, and SMC controller, have proposed a synchronous sliding mode control (SSMC) for a parallel robot model, tacking in the account the effect of dynamics uncertainties such as friction, external noise, and model error. The controller is designed based on the sliding surface to ensure that both tracking and synchronization errors converge towards zero simultaneously. The system's stability is confirmed using the Lyapunov theory. Figure (29) introduces an SSMC controller developed with a mode surface based on the cross-coupling error to force the system to perform synchronization.

$$s_2 = \lambda e^* + \dot{e}^* \tag{32}$$

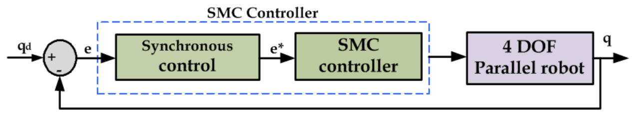

FIGURE 29. The SMC controller structure.

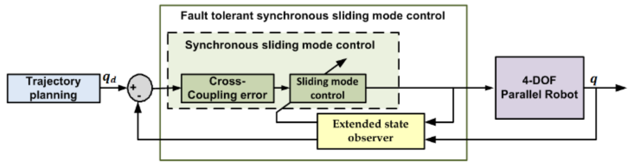

FIGURE 30. Diagram of the proposed control scheme.

where s_2 is the sliding variable, λ is the diagonal matrices which are definite positively [41].

Finally, the controller effects show better performance than traditional controllers such as PID, synchronous proportional-integral-derivative (SPID), and SMC controllers [41].

e: FAULT-TOLERANT SYNCHRONOUS SLIDING MODE

In 2024, Tran et al. [43] effectively employed a novel fault-tolerant synchronous sliding mode to control the 4-DOF parallel manipulator. This approach was designed to conquer uncertainties in the robot system, such as model errors and actuator faults. Furthermore, they rigorously employed the Lyapunov approach to theoretically validate the stability and robustness of the controller, effectively combining tracking and synchronous errors for optimal performance.

However, the cross-coupling error is considered a synchronous term that includes achieving tracking error toward zero. The system was improved using sliding mode control and the extended state observer (ESO) to address cross-coupling errors. This approach compensates for uncertainties, improving the controlled system's accuracy, stability, and robustness. The controlled system structure is shown in Figure (30).

The sliding variable is defined as follows:

$$s = \dot{E} + \lambda E \tag{33}$$

where λ presents a positive definite diagonal matrix.

To assess the benefits of the proposed control system in the robot, they compared the results with those of the PD controller, synchronous PD (SPD) controller, and synchronous sliding mode controller (SSMC). The results showed that better outcomes were achieved with the novel fault-tolerant synchronous sliding mode controller [43].

f: L_1 ADAPTIVE CONTROL

The L_1 adaptive controller outperforms the PD controller used by Bennehar et al. [40] to control the 4-DOFs, a parallel kinematic manipulator. The adaptive gain Γ can be increased without compromising the robustness of the closed-loop

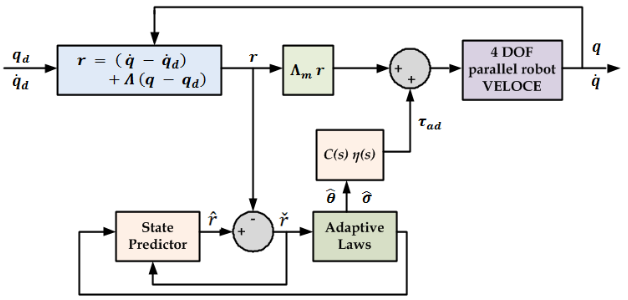

FIGURE 31. Block diagram of L_1 adaptive controller.

system. Notably, this control scheme offers a significant advantage with its model-free adaptive nature. In conclusion, the overall block diagram of the proposed L1 adaptive controller is clearly illustrated in Figure (31) [40].

Consider the combined tracking error r(t) as follows:

$$r = \left(\dot{q} - \dot{q}_d\right) + \Lambda\,(q - q_d) \tag{34}$$

In the given equation, Λ stands for a symmetric positive-definite matrix. The control input vector $\tau(t)$ comprises two distinct terms. The initial term is a fixed state-feedback component that defines the system's transient response, while the second term is an adaptive component that compensates for the system's nonlinearities.

$$\tau\,(t) = A_m r(t) + \tau_{ad}(t) \tag{35}$$

where the Hurwitz matrix A_m characterizes the system's transient response, while $\tau_{ad}(t)$ represents the adaptive component to be designed later [40].

The results indicated excellent tracking performance due to the compensation of nonlinearities in the adaptive controller [40].

g: ADAPTIVE CONTROL

Bennehar et al. [46] designed and demonstrated the effectiveness of the suggested L_1 adaptive controller for a 4-DOF fast parallel manipulator with the robot's inherent nonlinear dynamics are partially compensated for by additional dynamics-based terms.

Since L_1 adaptive control is inspired by Model Reference Adaptive Control (MRAC), firstly, MRAC is introduced for the investigated system. Subsequently, the construction of MRAC is modified to reach the decoupling of robustness and adaptation. Figure (32) clearly illustrates the principle of this control strategy.

The main distinction between MRAC and L_1 adaptive control is incorporating a prediction-based adaptive architecture. In the following discussion, we emphasize this new structure and show that it results in the same closed-loop behavior as direct MRAC. Figure (33) shows the summarized MRAC-based controller block diagram.

The proposed controller effectively compensates for the robot's inherent nonlinear dynamics, significantly reducing

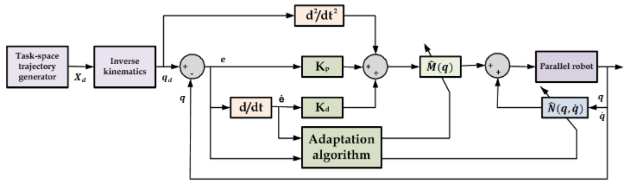

FIGURE 32. Block diagram of adaptive computed torque control.

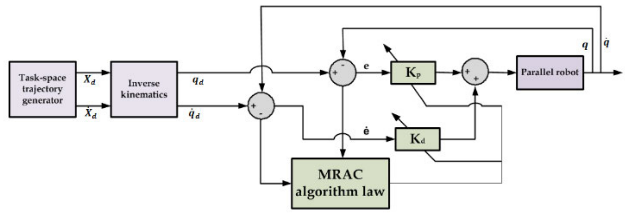

FIGURE 33. Block diagram of MARC.

uncertainties' impact on the closed-loop system and ultimately enhancing overall control performance [46].

h: ADAPTIVE TERMINAL SLIDING MODE CONTROL

Bennehar et al. [47] reached the advantages of relying on the desired trajectories instead of measured ones, which improves the proposed new adaptive controller based on terminal sliding mode (TSM) controller robustness and efficiency as applied on the 4-DOF parallel manipulator's robot called VELOCE [47].

This controller was supposed to be more robust and perform well. Also, it meets the requirements of those applications that need high precision, such as parallel manipulators [48]. Given that the dynamic parameters of the parallel manipulator are accurately known and no uncertainties exist (i. e. $\Gamma_d = 0$), the following control law can be chosen in order to ensure that e converges to zero in finite-time

$$\Gamma = Y\,(q,\dot{q},v)\,\theta - K_1 s - K_2\,|s|^{\rho}\,\mathrm{sign}(s) \tag{36}$$

where K_1 and K_2 are positive definite design diagonal matrices, $\rho < 1$ and the auxiliary control term v

$$v \triangleq \ddot{q}_d - \frac{1}{\beta_\gamma}\,|\dot{e}|^{2-\gamma}\,\mathrm{sign}(\dot{e}) \tag{37}$$

The control law assumes that the dynamic model is accurately known. However, in reality, the dynamic parameters of parallel manipulators may be unknown, uncertain, or changing over time (e.g. due to varying payload). While these variations can be handled as general disturbance terms, the fact that their structure is unknown can result in poor tracking performance, high feedback gain, and chattering [47].

Adaptive controllers are considered the most suitable solution to deal with uncertainties with known structure. Therefore, to take advantage of both adaptive control and terminal sliding mode, the best approach is to combine both terminal sliding mode and adaptive control into a single controller [47].

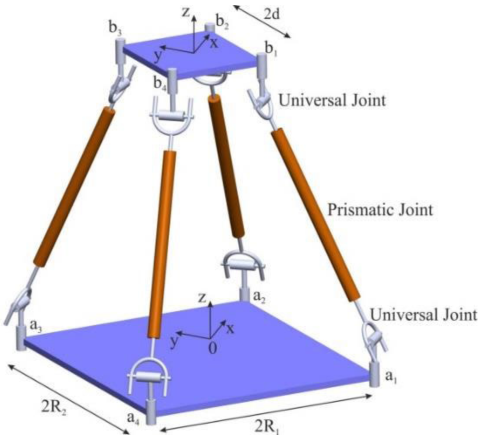

FIGURE 34. Scheme diagram of R4 parallel robot.

F. R4 REDUNDANTLY ACTUATED PARALLEL MANIPULATOR

Parallel manipulators with actuated prismatic joints have higher structural rigidity, better amplification, higher accuracy and precision trajectory tracking ability and positioning, as shown in Figure (34). The advantages of serial manipulators include higher dexterous workspace and simple forward kinematic relations pick-and-place operations. It has a backlash in their joints, higher friction, a large amount of noise and slow response [48].

1) DYNAMICS OF R4 PARALLEL ROBOT

During the robot's design phase, certain simplifications were made to determine the most efficient configuration in terms of performance and cost. These simplifications, such as ignoring joint friction, forearm inertia, and gravity acceleration, were strategic decisions. Half of the forearm mass is definitively transferred to the end of the arm, while the remaining half is transferred to the travelling plate [48].

The R4 robot is a redundantly actuated parallel manipulator with four actuators and three degrees of freedom. It is designed to achieve acceleration of up to 100G. The robot has a workspace at least the size of a cylinder with a 300mm radius and 100mm height. Each of its four motors can deliver a maximum torque of 127N•m. [26], [48], [49].

The final expression for the simplified forward dynamics of the robot is unequivocally derived from a combination of the travelling plate and the arm equilibriums. It is succinctly described by the following equation [26], [48], [49]:

$$\ddot{x} = \left(M_T + J_m^T I_T J_m\right)^{-1} J_m^T\left(\Gamma - I_T \dot{J}_m \dot{x}\right) \tag{38}$$

where $\dot{x} \in R^m$ and $\ddot{x} \in R^m$ are the vectors of Cartesian velocities and accelerations; $M_T = \mathrm{Diag}\left\{M_{tp} + n\frac{M_{foream}}{2}\right\}_{m\times m} = M_{tot} I_{m\times m}$ is a diagonal matrix with m diagonal terms, being M_{tp} the mass of the travelling plate, M_{foream} the mass of the forearm, M_{tot} the scalar value of the diagonal of M_T, m the number of degrees-of-freedom (m = 3) and n the number of motors (n = 4); $I_T = \mathrm{Diag}\{I_{act} + I_{arm}\}_{n\times n} = I_{tot} I_{n\times n}$ is an n diagonal terms matrix, the inertia of the actuators and the inertia of the arms are denoted as I_{act} and I_{arm}, respectively, and I_{tot} is the scalar rate of the diagonal of I_T; $J_m \in R^{n\times m}$ and $J_m \in R^{n\times m}$ represent the generalized inverse Jacobian matrix and its first derivative, respectively; and $\Gamma \in R^n$ represents the torques generated by the actuators [26], [48], [49].

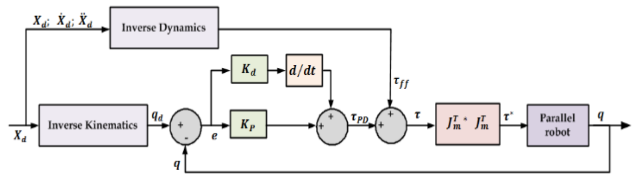

FIGURE 35. Block diagram of the proposed control scheme.

2) CONTROL SCHEMES FOR R4 REDUNDANTLY PARALLEL ROBOT

This part will briefly discuss the most important control strategies used for motion control of an R4 redundantly Parallel Robot, where designing the control for an R4 redundantly Parallel robot to carry out different processes is challenging. These controllers are Extended PD Control, Dual-Space Feedforward Control in the Cartesian Space, Dual-Space Feedforward Control, Dual Mode Adaptive Control, and Adaptive Control.

a: EXTENDED PD CONTROL

Bennehar et al. [50] proposed an extended version of PD controller for redundantly actuated parallel kinematic manipulators (Dual-V is a 3 DOF planar redundantly actuated parallel manipulator belonging to the 4-RRR family).

To further improve tracking performance by compensating for inherent nonlinearities, we can add a feed-forward term to partially compensate for the nonlinear dynamics. For the Dual-V robot, the feed-forward torque is computed as follows:

$$\tau_{ff} = J_m^T * M_I \ddot{X}_d + M_{II}\left(\dot{J}_m \dot{X}_d + J_m \ddot{X}_d\right) + \tau_3\left(X_d; \dot{X}_d; \ddot{X}_d\right) \tag{39}$$

where the subscript d refers to the preferred quantities. The structure of the system and controller is illustrated in Figure (35) [50].

The results were expected, as the primary goal of this paper is to present a technique for removing discontinuities from trajectories generated by classical analytical functions. These discontinuities are a significant cause of tracking loss [50].

b: DUAL-SPACE FEEDFORWARD CONTROL

Natal et al. [48] offered a dual-space adaptive controller for R4 redundantly actuated parallel manipulator for applications with excessive accelerations. Also, G. Natal et al. [51] also proved experimentally that applying a Dual-Space Feedforward PID Controller for R4 redundantly activated parallel manipulator.

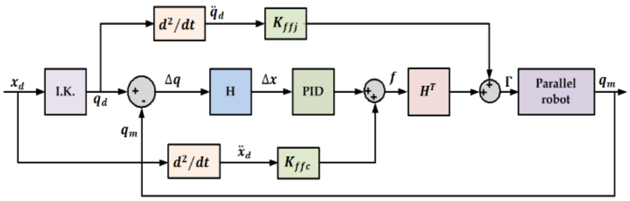

FIGURE 36. Block diagram of the proposed dual-space feedforward controller.

The dual-space feedforward controller consists of a PID in the Cartesian space, with feedforward of both desired Cartesian/joint accelerations to improve tracking performance. This control approach is illustrated in the block diagram of Figure (36).

They propose the implementation of the dual-space adaptive controller. Its general expression is given as follows:

$$\Gamma = \hat{M}(q)\,\ddot{q}_d + \hat{C}(q;\dot{q})\,\dot{q}_d + \hat{G}(q) + K_p e + K_d \dot{e} \qquad (40)$$

where $e = q_d - q$, $\hat{M}$, $\hat{C}$, $\hat{G}$ are the estimations of M, C and G (being M(q) the inertia matrix, $C(q;\dot{q})$ the vector of Coriolis and centrifugal forces, and G(q) the gravity vector), respectively [48], [51].

The results achieved by Natal et al. [48] demonstrate the dual-space adaptive controller's remarkable ability to compensate for load changes and its rapid response, making it suitable for high-acceleration pick-and-place tasks. Furthermore, it outperforms the dual-space feed-forward controller [48], showcasing its superior performance.

Natal et al. [51] found that the PID in Cartesian space had significantly superior tracking performance. They demonstrated excellent tracking performance even with a high acceleration of 40G (equivalent to over 425 pick-and-place cycles per minute). This was tested for spiral movements in the X-Y plane and 3D pick-and-place movements [51].

c: DUAL-SPACE FEEDFORWARD CONTROL IN THE CARTESIAN SPACE

Natal et al. [49] presented three types of controllers for R4 redundantly actuated parallel manipulator for applications with extremely high accelerations, which are: PID controller in the Cartesian space, The dual-space feed-forward controller, and Dual-space adaptive controller.

The proposed controller implemented on the R4 parallel manipulator is as follows:

1. PID controller in the Cartesian space

The main objective of PID was to consider the manipulator's actuation redundancy in the controller design; otherwise, critical internal forces may appear. This control scheme is illustrated in Figure (37) [49].

2. The dual-space feed-forward controller

This controller is essentially a PID in the operational space, enhanced by a feed-forward of both desired Cartesian and articular accelerations to significantly enhance its tracking implementation. This advanced control method is clearly shown in Figure (36) [49].

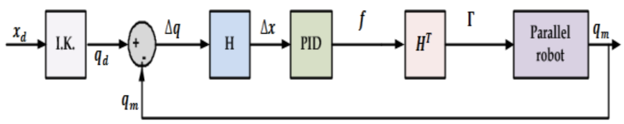

FIGURE 37. Cartesian PID controller block diagram.

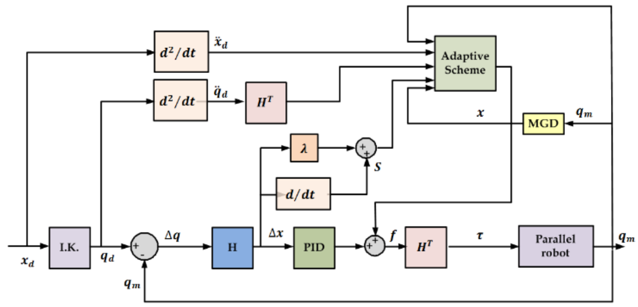

FIGURE 38. The proposed dual-space adaptive controller.

3. Dual - space adaptive controller

This controller, built on the dual-space feed-forward controller and adaptive control, is a marvel of engineering. Its key feature is its ability to consider the system's dynamics and automatically estimate its parameters in real-time, a feat that was once considered impossible [49]. The adaptive control system is outlined in the block diagram in Figure (38).

The results for the proposed controllers are as follows:

1. A PID controller functioning within a specific space will demonstrate subpar performance.

2. A dual-space feed-forward control system will deteriorate performance upon operational changes, such as payload variations.

3. The dual-space adaptive control scheme, with its consistent superiority over the aforementioned controllers, even when optimally tuned for specific cases, underscores its adaptability and effectiveness in industrial environments [49].

d: DUAL MODE ADAPTIVE CONTROL

A nonlinear dual-mode adaptive controller, known for its adaptability, was successfully implemented with very high accelerations in real-time for different scenarios. This work by Chemori et al. [26] showcases its effectiveness for both non-redundant parallel manipulators like the PAR2 robot, for 2D pick-and-place trajectories, and redundantly actuated parallel manipulators, for 3D pick-and-place trajectories.

The dual-space adaptive controller scheme extends the dual-space feed-forward controller shown in Figure (38). To greatly improve the control scheme's robustness, we have introduced an adaptation technique inspired by extending the dual-space feed-forward controller. The resulting scheme is called the "dual-space adaptive controller" and is thoroughly

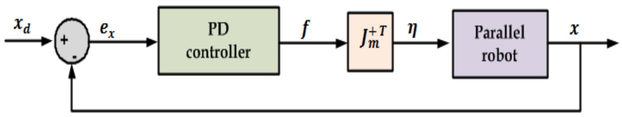

FIGURE 39. The PD controller in cartesian space block diagram.

explained in reference [26].

$$\Gamma = H^T \hat{M}_T \ddot{x}_d + \hat{I}_T \ddot{q}_d + K_p e + K_d \dot{e} \tag{41}$$

The given expression can be rephrased in Cartesian space as follows:

$$F = Y_r \hat{\theta} + K_p e_C + K_d \dot{e}_C \tag{42}$$

K_p and K_d are positive feedback gains, $e_C = x_d - x$, $\dot{e}_C = \dot{x}_d - \dot{x}$, and: $Y_r = \left[I_3 \times 3\ddot{x}_d \;\; J_m^T I_4 \times 4\ddot{q}_d \right]$; $\hat{\theta} = \begin{bmatrix} \hat{M}_{tot} \\ \hat{I}_{tot} \end{bmatrix}$

where Y_r and $\hat{\theta}$ the regressor vector and the considered parameters vector, respectively [26].

The experimental scenario unequivocally shows how to track a reference trajectory with an exceptionally high maximum acceleration [26].

e: ADAPTIVE CONTROL

Hussein [52] and Humaidi and Hussein [54] conducted two performance comparisons. The initial comparison assessed the performance of the PD controller in joint space versus the PD controller in Cartesian space. The second comparison assessed the performance of the Cartesian PD controller against adaptive controllers in terms of tracking and robustness of the R4 parallel robot. The adaptive controller was developed, and its stability was proven based on the Lyapunov theorem.

They started using a PD Controller that considers the parallel robot's actuation redundancy. Figure (39) illustrates the block diagram of the controller construction. X_d is regarded as the desired trajectory in Cartesian space, $X = [xyz]$ is the actual trajectory, and the inverse Jacobian matrix is denoted as J_m [52].

Secondly, Adaptive control is different from classical controllers because it has time-varying, not stationary, parameters. The adaptive control scheme unequivocally incorporates a PD feedback part and a whole dynamic feed-forward indemnification part while addressing the unidentified parameter of the manipulator and payload [52]. The control law and adaption law must be expressed in terms of sliding surface:

$$F = \hat{M}_{tot} \ddot{x}_r + J_m^T \hat{I}_{tot} \ddot{\theta}_r - K_D s \tag{43}$$

The controller's inputs consist of the desired Cartesian, each of position X_d, velocity $\dot{X}_d$, and acceleration $\ddot{X}_d$, along with the actual Cartesian position X and velocity $\dot{x}$. An illustration of the adaptive controller's structure can be found in Figure (40).

According to the findings, the PD controller in Cartesian space outperforms the PD controller in Joint space, with a 9.8% advancement. Additionally, the Cartesian adaptive controller shows even better tracking performance than the PD controller in Cartesian space, with a 45% advancement. Furthermore, it has been demonstrated that the Cartesian adaptive controller has better robustness characteristics, with a conflict of 0.078 mm, compared to the corresponding Cartesian PD controller [52].

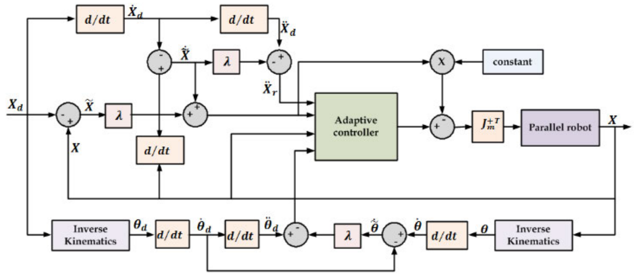

FIGURE 40. The adaptive controller in cartesian space structure.

In their 2019 study, Humaidi and Hussein [53] evaluated tracking performance by measuring the root mean square (RMS) value of Cartesian errors and assessed robustness by analyzing the variance of deviation in position response due to changes in the parameter. Additionally, the study included a stability analysis of the adaptive controller and demonstrated the global stability of the overall system in Cartesian space.

G. 5R PARALLEL ROBOT

The 5R symmetrical parallel mechanism consists of five bars connected end to end by five revolute joints. The optimal design of its mechanism involves two issues: performance evaluation (such as skillfulness, accuracy, stiffness, and activity index) and dimensional synthesis (link lengths). It can find a point position on a region of a plane known as the workspace, which has a limited workspace and difficulty with motion control due to singularity problems.

The restricted workspace size and the presence of singularities are major drawbacks of parallel robots. Numerous solutions have been proposed to address this issue [54]. This manipulator provides two degrees of freedom, enabling two independent Cartesian displacements at the end-effector through two active joints. It comprises two equivalent kinematic chains, denoted by the sub-index $i = 1, 2$. The fixed connection frame O is defined at the midpoint of A_1A_2, thus establishing the symmetry of the manipulator as $OA_1 = OA_2$, $A_1B_1 = A_2B_2$ and $B_1P = B_2P$. Each kinematic chain includes an active or actuated joint, a passive joint, and two links. The active joints are explicitly situated at point A_i, with their angular position precisely defined as θ_i. The passive joints are positioned at the end of each link connected to the active joints, designated as B_i.. Furthermore, the end-effector is specifically located at point $P(x, y)$ [55].

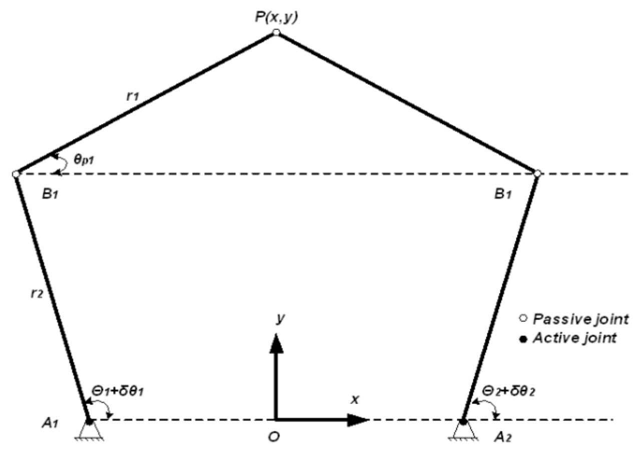

FIGURE 41. 5R symmetrical manipulator.

1) DYNAMICS OF 5 DOF PARALLEL ROBOT

The five-bar technique is a planar parallel technique comprising two actuators at the revolute joints in points A and E and three passive revolute joints in points B, C, and D, as depicted in Figure (41). The technique employed in this work has been meticulously designed to access all workspace positions without any collision between the proximal and distal legs [54].

This approach has calculated the robot's complete dynamic model. The model was identified using a weighted least squares method based on exciting trajectories combined with a classic geometrical control law. The identification resulted in the following model, which fully describes the robot dynamics of the studied mechanism [55]:

$$\tau = m_3 J^T \begin{pmatrix} \ddot{x} \\ \ddot{y} \end{pmatrix} + \begin{pmatrix} zz_1 \ddot{q}_1 \\ zz_2 \ddot{q}_2 \end{pmatrix} + \begin{pmatrix} f_{v1} \dot{q}_1 \\ f_{v2} \dot{q}_2 \end{pmatrix} + \begin{pmatrix} f_{s1} \mathrm{sign}(\dot{q}_{1)} \\ f_{s2} \mathrm{sign}(\dot{q}_2) \end{pmatrix} \tag{44}$$

where [54]:

- m_3 indicates the mass situated on the end effector.
- zz_1 and zz_2 signify rotational equivalent inertial terms on the first and second actuators.
- f_{s1} denotes the Coulomb friction term on the first actuator, and f_{s2} represents the same for the second actuator.
- f_{v1} represents the viscous friction term on the first actuator, while f_{v2} represents the same for the second actuator.

2) CONTROL SCHEMES FOR 5 DOF PARALLEL ROBOT

This part will discuss briefly the most important control strategies used for motion control of the 5 DOF Parallel Robot, where creating the control for a parallel robot to carry out different operations is incredibly challenging. These controllers are PI Control, Optimal PID Control, Anti-Windup Based PID Control, Feedback PID Control, and Computed Torque Control.

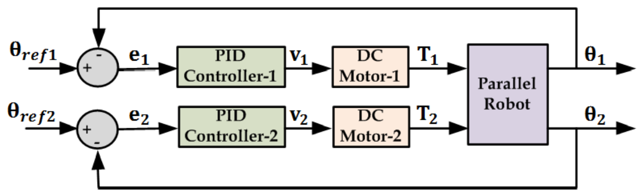

FIGURE 42. Block diagram of PID controller system.

a: PI CONTROL

PI controller for 5R parallel robot, which was designed by coupling SolidWorks and MATLAB software by Gohari et al. [56], as in the following equation:

$$P + \frac{1}{s} + D \frac{N}{1 + N\frac{1}{s}} \tag{45}$$

The controller result showed an acceptable path trajectory tracking with simulation and fabricated robot evaluation [56].

b: OPTIMAL PID CONTROL

In 2022, Sen et al. [57] rigorously applied three optimization procedures - genetic algorithm (GA), particle swarm optimization (PSO), and differential evolution (DE) - to a five-bar planar manipulator. They decisively determined the desired kinematic properties of the manipulator using inverse kinematics. Then, they framed an optimization problem aimed at minimizing shaking force and moments, with the desired kinematic quantities serving as rigorous constraints. Each optimization method relentlessly calculated the objective function until reaching the maximum number of iterations, ultimately identifying the best solution [57].

The manipulator's controller is crucial for practical applications, so we are focusing on designing a controller using the PID algorithm. The block diagram of this system is depicted in Figure (42). The kinetic energy, denoted as k, and the input torque equations T_i were derived as follows:

$$T_1 = K_1 \ddot{\theta}_1 + K_2 \ddot{\theta}_2 + K_3 \dot{\theta}_1^2 + K_4 \dot{\theta}_1 \dot{\theta}_2 + K_5 \dot{\theta}_2^2 \tag{46}$$

$$T_2 = l_1 \ddot{\theta}_1 + l_2 \ddot{\theta}_2 + l_3 \dot{\theta}_1^2 + l_4 \dot{\theta}_1 \dot{\theta}_2 + l_5 \dot{\theta}_2^2 \tag{47}$$

where the driving links' active joint angles are defined as $\theta 1$ and $\theta 2$, respectively [57].

The results indicate that:

1. The shaking force can be reduced by 99% and the shaking moment by 54%, significantly improving trajectory tracking accuracy.

2. The comparison demonstrated that the GA method outperformed the other methods using an equal number of iterations in the calculations [57].

c: ANTI-WINDUP BASED PID CONTROL

An improved PID with computed feedforward controller for a redundant parallel manipulator capable of executing a 5-DoFs (3T-2R) machining tool termed ARROW robot in a large

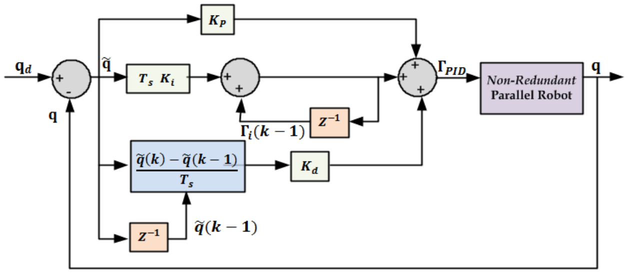

FIGURE 43. 5R The PID controller for a non-redundant parallel robot in joint space schematic block diagram.

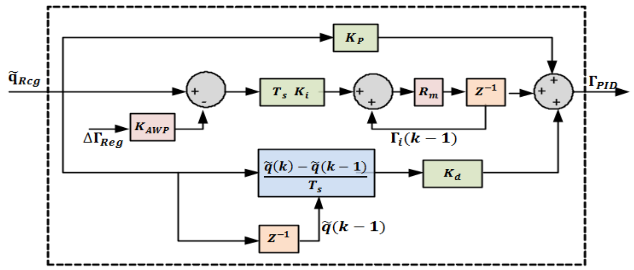

FIGURE 44. The schematic block diagram displaying a PID controller with a regularized integral term and an anti-windup strategy.

workspace with stating singularity analysis within the suitable workspace no existence for two types of singularities: constraint and classical singularity analysis were introduced by Saied et al. [58] they used a root mean square *for*error tracking with sufficient accuracy for a machining procedure [58].

They started by applying a PID controller, which is defined as a discrete for non-redundant parallel robot as in the following equations [58]:

$$\begin{cases} \Gamma_{PID}(k) = \Gamma_P(k) + \Gamma_I(k) + \Gamma_D(k) \\ \Gamma_P(k) = K_P\tilde{q}(k) \\ \Gamma_I(k) = \Gamma_I(k-1) + K_I T_s \tilde{q}(k) \\ \Gamma_D(k) = K_D\left(\frac{\tilde{q}(k)-\tilde{q}(k-1)}{T_s}\right) \end{cases} \tag{48}$$

At time step $\Gamma_P(k)$, $\Gamma_I(k)$, and $\Gamma_D(k)$ demonstrate the output torques or forces of the PID controllers, respectively. Meanwhile, K_P, K_I and K_D are diagonal positive definite matrix gains for the controllers. The joint position error vector, $\tilde{q} = q_d - q$, is defined as the difference between the desired position trajectory, q_d, and the measured position, q. T_s represents the sampling period. The PID controller for non-redundant parallel manipulators is illustrated in Figure (43) [58].

They proposed using the back-calculation approach with the PID controller block for the anti-windup strategy. This approach requires feeding back the difference between saturated and unsaturated signals, which may reduce the integral value as follows:

$$\begin{cases} \Gamma_I^{Reg}(k) = R_m(\Gamma_I^{Reg}(k-1) + K_I T_s(\tilde{q}_{Reg}(k) \\ \quad -K_{AWP}\Delta\Gamma_{Reg}) \\ \Delta\Gamma_{Reg} = \Gamma_{Reg}^{sat} - \Gamma_{Reg} \end{cases} \tag{49}$$

The forces or torques generated by the PID block for the saturation block in both after and before are represented by Γ_I^{Reg} and Γ_{Reg}, respectively. K_{AWP} is a diagonal positive definite matrix that denotes the anti-windup feedback gain. The schematic diagram illustrating the regularization technique of the integral term and the anti-windup strategy for the PID block can be found in Figure (44) [58].

Finally, they applied a PIDFF. which is compensation between PID added to a feed-forward part from the robot dynamics. The PIDFF control executed for the ARROW PKM can be expressed in joint space as follows:

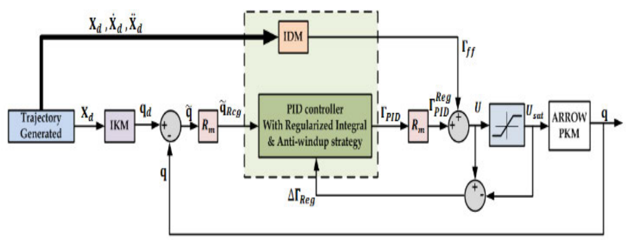

FIGURE 45. 5R ARROW PKM block diagram using PIDFF controller with regularizations and anti-windup strategy.

$$\begin{cases} U_{PM;T} = R_m\left(K_P\tilde{q} + \Gamma_I^{Reg} + K_P\dot{q}\right) + \Gamma_{PM;T_{ff}} \\ \Gamma_{PMff} = H_d^*\left(\ddot{x}_d^{PM} + \Lambda_d\dot{x}_d^{PM} - A_{Gd}\right) \\ \Gamma_{ff} = \begin{pmatrix} I_T/2 \\ -I_T/2 \end{pmatrix}\theta_{xd} \end{cases} \tag{50}$$

Γ_I^{Reg} represents the modified integral term, which includes the regularization and anti-windup strategy from equation (49). X_d^{PM}, $\dot{X}_d^{PM}$ and $\ddot{X}_d^{PM}$ are the desired position, velocity and acceleration of the moving platform, respectively. The matrices. H_d, Λ_d and A_{Gd} are used in the dynamic model of the parallel module and are calculated based on the desired generated trajectory. The vector $U_{PM;T}$ represents the control input forces applied to the linear actuators or torques to the rotative motors. θ_{xd} represents the desired rotation around the x-axis in Cartesian space. The proposed control solution for the ARROW PKM is explained in a schematic view in Figure (45).

An improved PID with computed feedforward controller after using a root mean square for error tracking with sufficient accuracy for a machining procedure [58].

d: FEEDBACK PID CONTROL

Righettini et al. [59] presented an investigation of 5R parallel industrial robot dynamic performance for its wide applications like pick-and- place and objects moving. They utilized the PD and PID control algorithms based on the inverse dynamics control, incorporating integral action within the task space inverse dynamics controller (TSIIDC). The centralized control systems are established on task space

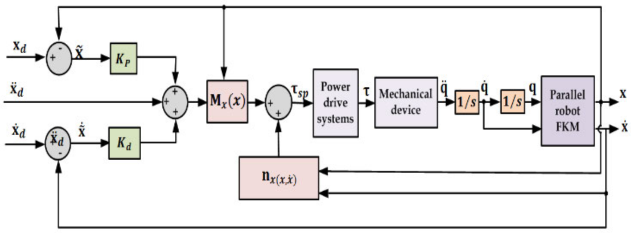

FIGURE 46. **The inverse dynamics task space controller schematic.**

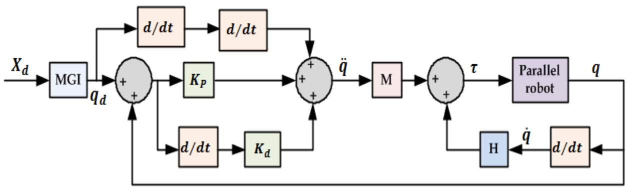

FIGURE 47. **Computed torque control law.**

variables, which allow the designer to directly specify the desired dynamics of the end-effector position error, $\tilde{x} = x_d - x$ (where x_d represents the setpoint and x represents the end-effector position). Figure (46) depicts one such controller, the task space inverse dynamics controller (TSIDC) [59].

The torque setpoint is determined based on the following equation using diagonal matrices K_p and K_d:

$$\tau_{sp} = M_x(x)\left(\ddot{x}_d + K_d\dot{\tilde{x}} + K_p\tilde{x}\right) + n_x(x,\dot{x}) \tag{51}$$

The results show significantly lower RMS errors and the effectiveness of tracking even with complicated high-speed trajectories in an industrial application [59].

e: COMPUTED TORQUE CONTROL

Pagis et al. [54] introduced three various types of singularities: Type 1 (serial) singularities, Type 2 singularities or parallel singularities, and Type 3 singularities for Five-bar planar parallel mechanism, where they proposed both Computed Torque Control (CTC) and Multi-model control law, then they concentrated on controlling the robot to pass the Type 2 singularities in the absence of any torque abruption. The proposed control law is then combined with an optimal trajectory planning method to enhance robustness to modelling errors and ensure perfect trajectory tracking by the robot.

Consequently, CTC computes the input torques in the following equation:

$$\tau = \mathrm{M}\left(\ddot{q}_d + K_d\dot{e} + K_p e\right) + \mathrm{H}(q,\dot{q}) \tag{52}$$

It's important to have the position vector x in task space to calculate the matrices M and H. However, in most cases, mechanisms have sensors that measure the position vector q in joint space q, as illustrated in Figure (47).

FIGURE 48. **The HEXA 6 DOF parallel robot.**

The results undeniably demonstrate the robustness and relevance of the controller devoted to crossing Type 2 singularities in parallel robots [54].

H. HEXA ROBOT IS A 6-DOF PARALLEL ROBOT

The actuators are positioned outside the workspace or fully isolated from it, which significantly improves performance. Its minimal number of moving links in the working area enhances its functionality, making it suitable for various applications such as medical robots, positioning devices, machine tools, and additive manufacturing systems.

The HEXA robot boasts a fully parallel robot structure with six degrees of freedom, guaranteeing high stiffness, accuracy, dynamic behavior, and efficient payload capacity, as illustrated in Figure (48) [2].

There are several limitations, such as:

It seems to be less rigid than the traditional manipulators

It is not well appropriate for high-speed operation.

It also has complicated control because of the presence of wires.

1) DYNAMICS OF HEXA 6 DOF PARALLEL ROBOT

A six-degree-of-freedom parallel kinematic machine has the very difficult task of measuring the robot end effector, a very expensive

In addition, a 6-DoF PKM robot has complex dynamics that lack an analytical solution. The nonlinearity of the actuation systems further compounds this complexity. Therefore, to establish a control strategy, it is crucial to transform the dynamic equations into a linear form, as shown below:

$$T_m = M(q)\,\ddot{q} + f(q,\dot{q}) \tag{53}$$

In the given equation, motor torques are represented by the T_m vector, and the joint positions are represented by the q vector. M (q) is both symmetric and positive manipulator matrix definite of mass. The vector $f(q,\dot{q})$ accounts for the force or the torque resulting from centrifugal, Coriolis, gravity, and friction forces [60].

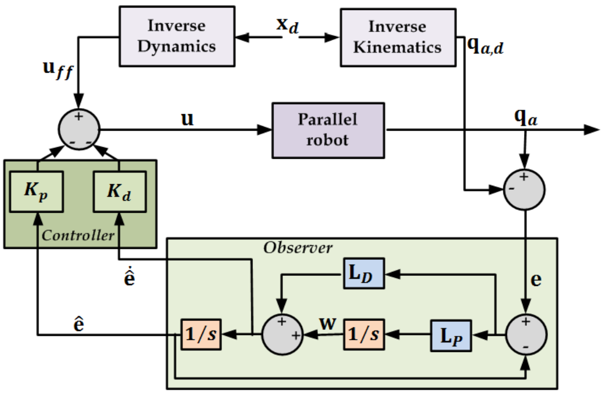

FIGURE 49. Proposed combined controller concept.

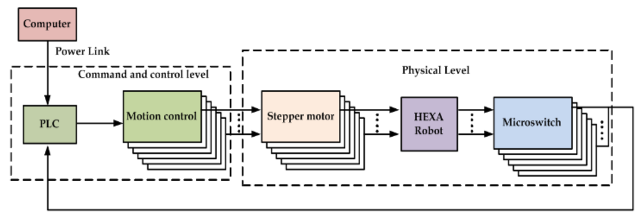

FIGURE 50. The control system of the HEXA robot.

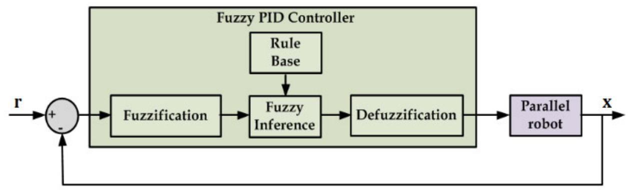

FIGURE 51. The block diagram of fuzzy PID type controller.

2) CONTROL SCHEMES FOR 6 DOF PARALLEL ROBOT

This part will briefly discuss the most important control strategies used for motion control of the 6 DOF Parallel Robot, where developing the control for a 6 DOF Parallel robot to implement different processes is challenging. These controllers are Model-Based Control, PLC – Based Control Architecture, Fuzzy PID Control, Adaptive Position-Force Control, Adaptive Admittance Control, and Robust Nonlinear Adaptive Control.

a: MODEL-BASED CONTROL

Abdellatif et al. [61] presented and discussed perfect and computationally efficient modelling of the dynamics of 6-DOF parallel robots called the PaLiDA robot. They then proposed a model-based controller for robust *design* of controller-observer for the single actuators. As shown in Figure (49), it is composed of three parts: a feed-forward part (generating desired forces u_{ff}), a linear feedback controller, and a linear observer [62].

$$\text{controller}:\begin{cases} u = u_{ff} + u_c \\ u_c = -K_D\dot{e} - K_P\hat{e} \end{cases} \tag{54}$$

$$\text{observer}:\begin{cases} \dot{e} = w + L_D(e-\hat{e}) \\ \dot{w} = -L_P(e-\hat{e}) \end{cases} \tag{55}$$

where, K_P represents the controller proportional gain, K_D is the derivative gain, L_P stands for the observer proportional gain, L_D is the observer derivative gain, and e represents the controller error. These gains are all considered to be positive, similar to those of the parallel robot [61].

A centralized feedforward dynamics compensation enhances it. Since systematic tracking errors always remain, a model-based iterative learning controller is designed to increase the accuracy at high dynamics [61].

b: PLC – BASED CONTROL ARCHITECTURE

A new control architecture for the six degrees of freedom HEXA parallel robot is presented by Vaida et al. [62], which was divided into three levels: User level, Command and control level, and Physical level. The robot's PLC now has a control algorithm that enables real-time control of complex movements, ensuring the safe operation of the HEXA robot. The new control system uses the communication system POWERLINK and the programming standard PLC Open, allowing for the creation of a standardized control structure for any 6-axis robotic system [62]. The schematic of the HEXA robot control and actuation system representation is shown in Figure (50).

c: FUZZY PID CONTROL

Babaiasl et al. [63] implemented a fuzzy PID controller for Hexa robot is a 6-DOF parallel robot, where the fuzzy PID controller is used for trajectory tracking and convergence of error to zero, which contains the advantages of both PID and fuzzy controllers. The general structure of fuzzy logic control is represented in Figure (51) and comprises three principal components: Fuzzification, Rule base, and Defuzzificatio [63].

The results show good time and precision response when these parameters are well adjusted by fuzzy logic compared with the results obtained from the classical PID controller, where the position error was decreased by 30% with the addition of the fuzzy controller [63].

d: ADAPTIVE POSITION-FORCE CONTROL

Jos'e Puglisi [64] developed all the concepts and experiences involved in controlling a 6 DOF Hydraulic Parallel Manipulator after actuators are modelled and experimental identified. Both traditional PID controllers are presented, and the PI+P adaptive controller is implemented. The last controller strategy for the PM is developed, and its performance is analyzed using simulation. The general architecture of this controller is clearly presented in Figure (52). The first two blocks in the diagram definitively correspond to trajectory generation. The PI+P adaptive position-force controller has been effectively implemented based on this architecture. It was significantly

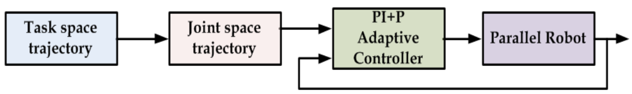

FIGURE 52. Schematic diagram for the joint space controller.

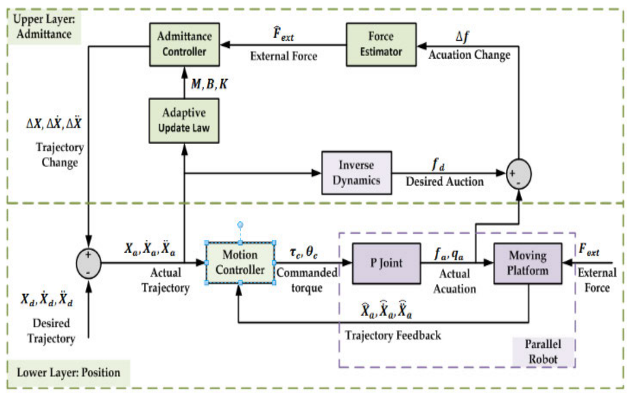

FIGURE 53. Adaptive admittance controller scheme of the 6 DOF parallel robot.

modified to efficiently receive information from the force sensor integrated into the PM [64].

They applied the integral absolute error (IAE), and the results showed better controller tracking response in both peaks and valleys of the target position [64].

e: ADAPTIVE ADMITTANCE CONTROL

To achieve human-robot collaborative (HRC) assembling of significant, heavy components without using external sensors, Sun et al. [65] applied a sensorless adaptive admittance controller the dynamic model of a six-degree-of-freedom (6 DOF) parallel robot based on finite and instantaneous screw (FIS) theory, which adopted to convert the change of estimated force to the change in position, velocity and acceleration, it was designed by using robot velocity as reference. Figure (53) The lower layer is a position controller based on inverse kinematic of the 6-DoF parallel robot.

The results unequivocally demonstrate the accurate estimation of external force. The robot effortlessly complies with the operator's force and successfully achieves adaptive admittance control, thereby significantly enhancing the execution time and accuracy of the HRC assembly [65].

f: ROBUST NONLINEAR ADAPTIVE CONTROL

A mathematical model of ball-screw drive actuators and Hexaglide Robot, which is a 6-degree of freedom (DOF) parallel robot with prismatic actuated joints, is used as an application case considered by Negahbani et al. [60] where considering the most influencing sources of nonlinearity: sliding-dependent flexibility, backlash, and friction. Finally, a nonlinear adaptive-robust control algorithm for trajectory tracking is described and simulated based on minimizing the tracking error. Figure (54) depicts the proposed controller block diagram [60].

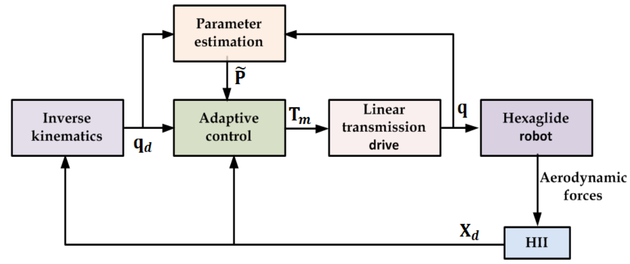

FIGURE 54. The adaptive-robust controller for the HEXAGLIDE robot block diagram.

An action controller can be obtained using an appropriate motor torque input, described in the following equation:

$$\mathrm{T_m} = \Psi\left(\mathrm{q}, \dot{\mathrm{q}}, \dot{\mathrm{q}}_\mathrm{r}, \ddot{\mathrm{q}}_\mathrm{r}\right)\mathrm{p} + \mathrm{K_D}\mathrm{s} + \mathrm{K_I}\int \mathrm{s}\mathrm{ds} + \eta\,\mathrm{sat}(\phi^{-1}\mathrm{s}) \quad (56)$$

This equation, Ψ, represents a matrix containing nonlinear equations, and p is a vector containing dynamical parameters. Furthermore, $\mathrm{K_D}$, $\mathrm{K_I}$, η, and Φ are positively diagonal matrices. The position error vector of the sliders is unambiguously defined as $\mathrm{e} = \mathrm{q_d} - \mathrm{q}$, where $\mathrm{q_d}$ denotes the preferred position of the slider derived via inverse kinematics from the preferred platform pose. The vector s unambiguously describes the combined error [60].

The work's results show that the ball-screw linear actuator with PID adaptive-robust control can achieve an accuracy of about 0.7 mm in TCP position and 0.17 degrees in platform orientation. These results match our performance requirements and confirm the design choices for the actuation system and control algorithm strategy [60].

I. CABLE-DRIVEN PARALLEL ROBOTS (CDPRS)

Cable-driven parallel robots (CDPRs) have garnered considerable attentiveness recently due to their advantageous features. In these parallel robots, rigid links are replaced by multiple parallel cables [66]. CDPRs use cables as the transmission element. They have the advantages of simple structure, large load/mass ratio, spacious workspace, and strong carrying capacity, as shown in Figure (55).

These robots possess many applications, including instrumentation, medical rehabilitation, heavy object transportation, hazardous area clearance, comprehensive workspace utilization, lifting, aircraft wind tunnel testing, construction, and 3D printing [67]. Cable robots' lack of rigid links creates structural challenges [67]. Rod-supported series robots find these tasks challenging. Cable-driven parallel Robots (CDPRs) are considered difficult according to their highly nonlinear dynamic behaviour, significant uncertainties, low-stiffness cables, parameter interpretation, cable stresses, and actuation redundancy.

The advanced design of CDPRs, with their lower mass and improved rigidity, significantly reduces the impact of

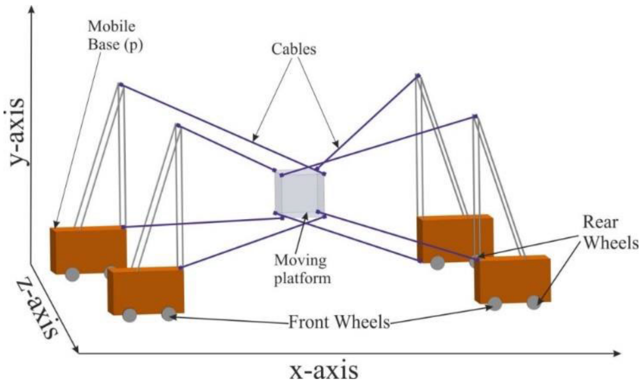

FIGURE 55. The Cable-driven parallel robots (CDPRs).

environmental noise on the robot, which is considered an advantage over other parallel robots [67].

1) DYNAMICS OF CABLE-DRIVEN PARALLEL ROBOT

Cable-driven parallel robots (CDPR) comprise a mobile platform (end-effector) connected to a fixed base using flexible cables. Winches control the lengths of the cables, enabling the platform to move. The cables can be unwound over long distances, consenting for a huge workspace. This, coupled with the cables' ability to carry heavy payloads, makes CDPR well-suited for tasks that require the manipulation or positioning of large objects [68].

The workspaces in parallel cable robots are divided into four main groups: available workspace, static workspace, dynamic workspace, and controllable workspace [67].

The following equation represents the dynamic model of the cable robot:

$$M(x)\ddot{x}+C(x,\dot{x})\dot{x}+N(x,\dot{x})+T_d=J^TK(L_2-L_1) \quad (57)$$

$$I_m\ddot{q}+rK(L_2-L_1)=u_r+K_v\left(\dot{L}_2-\dot{L}_1\right) \quad (58)$$

in which,

$$N(x,\dot{x})=G(x)+F_d\dot{x}+F_s(\dot{x}), \quad (59)$$

$$L_2=rq+L_0 \quad (60)$$

Let x be the robot's position vector, M(x) be the mass of the robot, and $C(x,\dot{x})$ denote Coriolis and centrifugal expressions. Similarly, G(x) represents the gravity term, F_d signifies the viscosity friction coefficient matrix, F_s denotes the Columbine friction matrix, and T_d stands for turbulence. Additionally, L_2 and L_1 correspond to the length and the voltage of the cable length vectors. An approximation can be obtained by solving the robot's inverse kinematic problem, L_0 representing the cable length vector at $x = 0$, and j representing the Jacobin matrix. Furthermore, q is the actuators' angular vector, I_m denotes the inertia coefficient matrix, and u represents the torque vector input. r is the actuator radius, and K is the cable stiffness matrix [67].

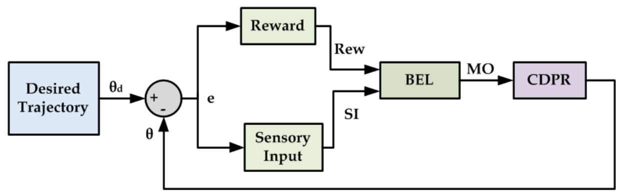

FIGURE 56. BEL's network model algorithm.

Now, the variable $z = K(L_2 - L_1)$ is tacked into the account, and it is assumed that K_v and K are in the order of $O(1/\epsilon_p)$ and $(1/\epsilon_p^2)$, respectively [66].

When the cables are subject to tensile forces, it is crucial to ensure the controller maintains cable tension across the whole workspace. This is vital for the robot's stability and performance, as any slack in the cables can lead to unpredictable movements and potential safety hazards.

2) CONTROL SCHEMES FOR CABLE-DRIVEN PARALLEL ROBOT

This part will briefly discuss the most important control strategies used for motion control of a Cable-driven parallel Robot, where designing the controller for a Cable-driven Parallel robot to performed different operations is challenging. These controllers are Brain Emotional Learning-Based Intelligent Control, Nonlinear Model Predictive Control, Fuzzy Logic – Based Sliding Surface Control, Dual-Space Feedforward Control, LQ Optimal Control, Adaptive Fuzzy Control, Rise Feedback Control, and active fault-tolerant hybrid Control robust fault-tolerant Control, and adaptive passivity-based control

a: BRAIN EMOTIONAL LEARNING-BASED INTELLIGENT CONTROL

Bajelania et al. [69] used the Brain Emotional Learning-Based Intelligent Controller (BELBIC), which is a bio-inspired intelligent approach to overcome these challenges for a plotter Cable-Driven Parallel Robots CDPR. Moreover, BEL's network model algorithm is depicted in Figure (56).

This network uses two input signals: Sensory Inputs (SI) and reward (Rew). The network's output is the difference between these signals, interpreted as the control effort in the Amygdala and the Orbitofrontal Cortex. Learning takes place as both the reward and the SI modify the gains in the Amygdala and the Orbitofrontal Cortex at each time step.

The saturation functions are employed to define the learning functions as equations below. This ensures that the learning signals are kept within limits and the cable forces remain positive. The following equations illustrate that the controller is entirely designed in joint space, negating the need for the Jacobian matrix [69].

$$Rew=\left(1+\exp(a_{Rew}(K_{1_{Rew}}e+K_{2_{Rew}}\frac{de}{dt}))\right)^{-1} \quad (61)$$

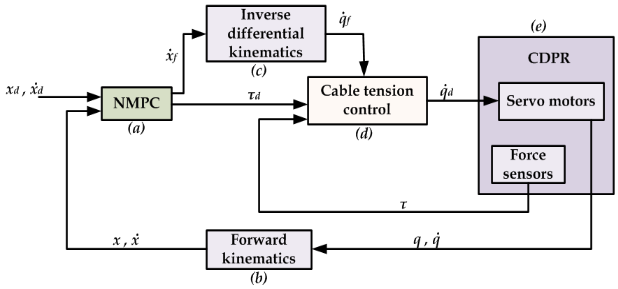

FIGURE 57. The Block diagram of a position tracking control scheme integrating the proposed NMPC.

$$\mathrm{SI} = \left(1 + \exp(a_{SI}(K_{1SI}e + K_{2SI}\frac{de}{dt} + K_{3SI}\int edt))\right)^{-1} \tag{62}$$

The conclusions suggest that BELBIC could be utilized as a new method for solving the trajectory tracking issue in CDPRs. It can achieve a satisfactory tracking error (less than 10 degrees) without the need to utilize the Jacobian matrix in the feedback loop [69].

b: NONLINEAR MODEL PREDICTIVE CONTROL

Santos et al. [70] controlled six degree-of-freedom Cable-Driven Parallel Robots (CDPRs) by applying a Nonlinear Model Predictive Control (NMPC) strategy for the position tracking the concept of Wrench Equivalent Optimality (WEO) is a non-negative-measure-that can evaluate whether the wrench generated by a given cable tension vector can be generated by an alternative tension vector with a smaller 2-norm [70].

The block diagram in Figure (57) outlines an overall position-tracking control scheme integrating the NMPC strategy.

As a result, the tracking accuracy was substantially reduced compared to a previously introduced LMPC scheme [70].

c: FUZZY LOGIC – BASED SLIDING SURFACE CONTROL

A supervisory interval type-2 fuzzy adaptive sliding mode controller (SIT2FASMC) by Aghaseyedabdollah et al. [66] to reach the cable parallel robot's desired performance even with the cables' vibration modes. They employed the singular disturbance theorem to analyze the vibration effects of elastic cables and conclusively confirmed stability using the second Lyapunov method. They unequivocally proposed an interval type-2 fuzzy logic controller to adjust the control gain, decisively reducing the chattering level. This controller was also introduced to regulate the gains within the sliding surface steadfastly. Additionally, a Grasshopper Optimization Algorithm was rigorously used to select the optimal parameters for the membership functions of the fuzzy system, as shown in Figure (58) [66].

The simulations demonstrate that the desired tracking performance is achieved despite uncertainties in the cable robot's parameters and structural constraints [66].

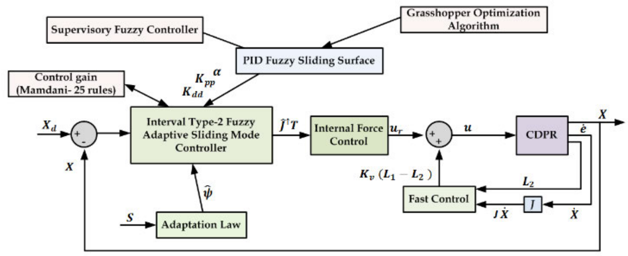

FIGURE 58. The block diagram illustrates the supervisory interval type-2 fuzzy adaptive sliding mode control optimized by the GOA.

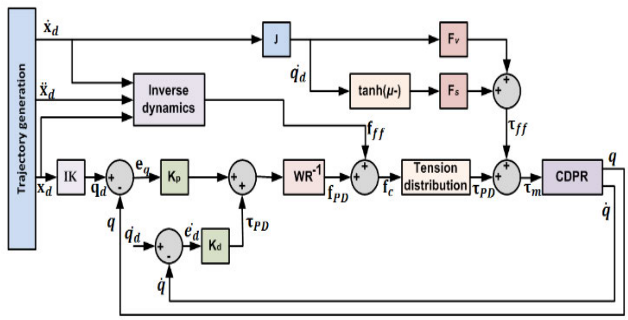

FIGURE 59. The Dual-space feed-forward control scheme with joint space controller.

d: DUAL-SPACE FEEDFORWARD CONTROL

In 2013, Lamaury et al. [68] achieved improved tracking performance on a large redundantly actuated CDPR prototype by implementing an adaptive dual-space motion control method. This approach aimed to enhance the robot's tracking capabilities while maintaining tension in all the cables, even in the presence of uncertainties and changes in the robot's dynamic parameters.

The dual-space feed-forward control structure offered in Figure (59) is proposed with a PD controller joint space, where the overall control law is written as:

$$\tau_m = \tau_{ff} + RW^{+}f_{ff} + RN\lambda + RW^{+}WR^{-1}(K_p e_q(t) + K_d \dot{e}_q(t)) \tag{63}$$

where the feed-forward terms τ_{ff}, $f_{ff} = M(x)\ddot{x}_d + c(x,\dot{x})\dot{x}_d - f_g(x)$ compensates for the platform dynamics *and* $f_{ff} = WR^{-1}(K_p e_q(t) + K_d \dot{e}_q(t))$ tracks the desired trajectory. It is crucial to note tha tK_p *and* K_d represent positive definite gain matrices. Additionally, e_q is the error vector of rotational position actuator $e_q = q_d - q$ *and* $\dot{e}_q$ the error vector of rotational speed actuator $\dot{e}_q = \dot{q}_d - \dot{q}$ [68].

The dual-space adaptive control is represented by applying two corrective feed-forward terms in the framework of the dual-space adaptive control scheme shown in Figure (60). The variations and uncertainties, which act as disturbances on the closed-loop system, can seriously impact the controller's performance. The suggested adaptive control law is precisely defined as:

$$\tau_m = Y_{q_r}(\dot{q}_r)\,\hat{\theta}_q + RW^{+}Y_{x_r}(x, \dot{x}, x_r, \dot{x}_r)\hat{\theta}_x$$

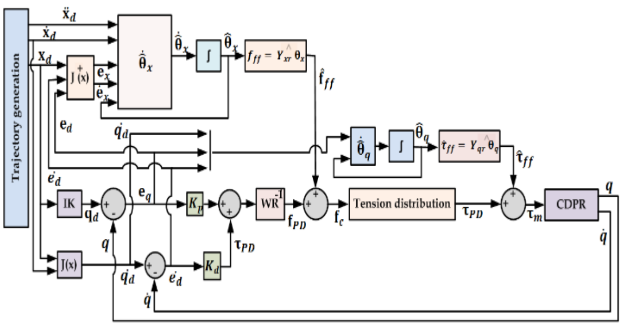

FIGURE 60. The Dual-space controller with joint space controller schematic.

$$+\mathrm{RN}\lambda+\mathrm{RW}^{+}\mathrm{WR}^{-1}(\mathrm{K_p e_q(t)}+\mathrm{K_d}\dot{\mathrm{e}}_\mathrm{q}(\mathrm{t})) \quad (64)$$

The reference velocities $\dot{x}_r$ and accelerations $\ddot{x}_r$ are defined as $\dot{x}_r = \dot{x}_d+\lambda e_x$ and $\ddot{x}_r = \ddot{x}_d+\lambda\dot{e}_x$, respectively. Here, e_x and $\dot{e}_x$ denote the position and velocity operational space errors and matrix Y_{x_r} denotes the known functions of the gravity action [68].

The experiments undeniably demonstrate the effectiveness of the proposed adaptive controller and the significant impact of the feed forwards on the performance of the closed-loop controlled system [69].

e: LQ OPTIMAL CONTROL

Abdolshah et al. [71] employed a linear quadratic (LQ) optimal controller for both the static and dynamic modelling of a 3-DOF planar cable-driven parallel robot (Feriba-3). They also proved that applying the LQ optimal controller makes the system track the reference efficiently with very low error and the system ensures high-quality trajectory tracking for both circular and trapezoidal trajectories in terms of displacement and velocity [71].

The objective is to observe W(t) as the controller function to minimize the performance index J, which is the system's integral output variables of a quadratic function y(t) and the control function W(t). Nevertheless, there may be errors in motion. The implementation index is described as follows [71]:

$$\begin{aligned} J &= \int_0^\infty \left[y^T(t).Q.y(t) + W^T(t).L.W(t)\right] dt \\ &= \int_0^\infty \left[q^T(t).C^T.q(t) + W^T(t).L.W(t)\right] dt \end{aligned} \quad (65)$$

where Q and L are weighting matriculated to the system output and control input, respectively. If the system's input is considered the output results of linear feedback, the following equation can be expressed:

$$W(t) = -K.C.q(t) \quad (66)$$

where the optimal value of K is obtained by $K = L^{-1}.B^T.P$ and P is attained by applying Riccarti's equation [71].

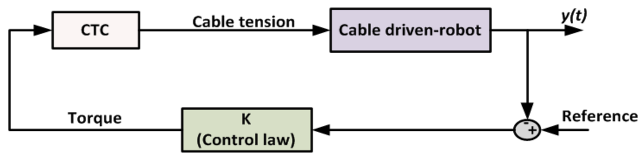

FIGURE 61. Block diagram of the control system.

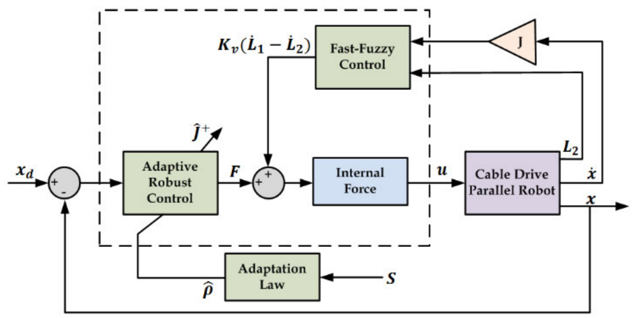

FIGURE 62. Proposed controller block diagram.

Figure (61) shows the designed controller system block diagram.

f: ADAPTIVE FUZZY CONTROL

Vu et al. [67] have developed an adaptive fuzzy controller for a cable-driven parallel robot (CDPR). The results unequivocally demonstrate that the system's accuracy in tracking the reference value and the controller's speed outperforms the robust method.

The controller block diagram in Figure (62) comprises an adaptive robust controller, fast-fuzzy control, adaptation law, cable-driven parallel robot, and inner force blocks.

The adaptive robust controller uses the sliding surface S for designing the coefficient (ρ^i) through adaptation laws. The fast-fuzzy control block employs fuzzy rules to calculate specific parameters of the adaptive robust controller. The resulting adaptive, fast-fuzzy controller is then implemented on (CDPR). A feedback loop compares the state variables x of (CDPR) with the preferred trajectories x_d at every moment [67].

In one of the simulation modes, the control system's intersection performance speed is diminished, with a tiny error, demonstrating the adequate performance of the proposed adaptive fuzzy method [67].

g: RISE FEEDBACK CONTROL

Hassan et al. [72] successfully used a Robust Integral of the Sign of the Error (RISE) control scheme. The RISE Feedback Controller (RISE) is a robust, nonlinear, continuous controller that ensures semi-global asymptotic search with restricted system structure supposition. It unequivocally guarantees the robustness of the closed-loop system against parametric uncertainties and exterior disturbances for the

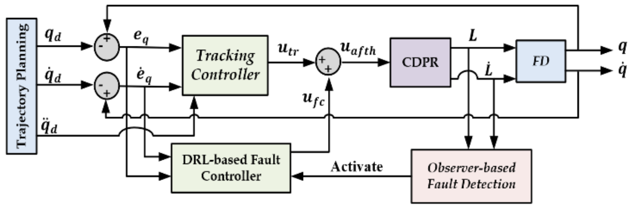

FIGURE 63. The Structure of active fault-tolerant hybrid control AFTHC for CDPR.

4-DOF Cable-Driven Parallel Robot (CDPR) called PICK-ABLE. The RISE control law is expressed as follows:

$$\Gamma_{\mathrm{RISE}} = (\mathrm{K_s}+1)\,\mathrm{e_2}(\mathrm{t}) - (\mathrm{K_s}+1)\,\mathrm{e_2}(\mathrm{t_0}) + \int_{\mathrm{t_0}}^{\mathrm{t}} [(\mathrm{K_s}+1)\,\alpha_2 \mathrm{e_2}(\sigma) + \beta \mathrm{sgn}(\mathrm{e_2}(\sigma))]\mathrm{d}\sigma \quad (67)$$

where $\mathrm{K_s}$, α_2, β are positive control design parameters, $\mathrm{t_0}$ is the initial time and sgn(:) is the standard signum function. Using the RISE controller, a TD algorithm should be integrated into the control law [71] to control a CDPR.

The results indicate that the proposed controller performs better than the classical PID controller and the first-order Sliding Mode Control (SMC) regarding tracking performance and robustness towards payload variations [72].

h: ACTIVE FAULT-TOLERANT HYBRID CONTROL

Lu et al. [72] developed the Active Fault-Tolerant Hybrid Control (AFTHC) system for cable-driven parallel robots (CDPRs). This system utilizes deep reinforcement learning (DRL) to handle actuator uncertainties and includes a performance tracking mechanism, a Fixed-Time Sliding Mode Observer (FTSMO) for fault detection, and a DRL-based controller for fault compensation. Its aim is to enhance stability and quickly restore control performance after a fault is detected. Thus, the cost function $ca(n)$ for the MDP was designed as the following equation:

$$c_a(n) = e_q^T(n)\,K_{c1}e_q(n)\,e_L^T(n)\,K_{c2}e_L(n) + f_{co}(n) \quad (68)$$

where K_{c1} and K_{c2} are the coefficient matrices. e_L denotes the tracking error vector of cable lengths. $f_{co}(n)$ is the constrained function.

The AFTHC scheme flow diagram shows that the tracking controller manages the system while fault detection monitors it as shown in figure (63) [72].

The DRL-based AFTHC system features a fault detection module and compensation controller, quickly restoring control accuracy during sudden actuator faults, outperforming traditional fault-tolerant methods [73].

i: ROBUST FAULT-TOLERANT CONTROL

Fazeli et al. [74] developed a strong control method to keep the cables of a cable-driven parallel robot under positive tension. This method works effectively even when there are actuator faults or uncertainties in the system. They used a type of control called adaptive finite-time sliding mode control along with a nonlinear adaptive observer, as shown in Figure 64. Generally, redundancy resolution methods, which started as optimization techniques, help maintain even tension distribution in redundant cable-driven parallel robots (CDPR).

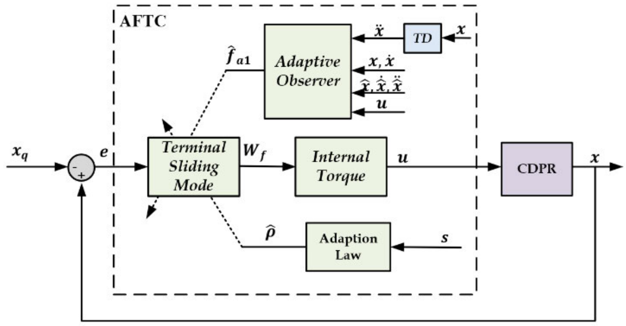

FIGURE 64. The Structure of an adaptive feedforward-based control for CDPR with an ISP controller.

Controlling the system is challenging due to uncertainties in redundancy resolution (RR) techniques. This approach identifies uncertainties and faults in actuators, while the controller corrects errors in the observer's estimates. The proposed observer ensures stability through H∞ stability using linear matrix inequality. We also demonstrate that the system remains stable in finite time using Lyapunov's methods.

Experimental validation of the proposed scheme's performance was conducted in the presence of actuator defects and model uncertainties using a planar CDPR [74].

j: ADAPTIVE PASSIVITY-BASED CONTROL

Cheah et al. [75] proposed a novel adaptive feedforward-based controller to establish a passive input-output mapping for the CDPR, which is used with a linear time-invariant strictly positive real feedback controller to ensure robust closed-loop input-output stability and asymptotic pose trajectory tracking via the passivity theorem. The controller is being developed for application with various payload attitude parameterizations, including any unconstrained attitude parameterization, the quaternion, or the direction cosine matrix (DCM). The proposed control input is described by:

$$F = f_{ff} + f_{fb}, \quad (69)$$

where f_{ff} is an adaptive feedforward-based input and f_{fb} is a feedback input.

The CDPR utilizes an adaptive feedforward-based control input along with pretension and force distribution, as illustrated in the block diagram shown in figure (65). This system has been demonstrated to be passive, incorporating negative feedback with an ISP controller [75].

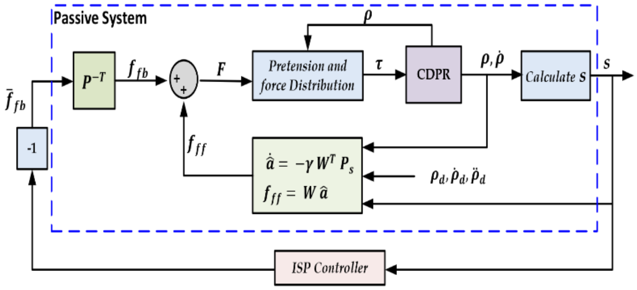

FIGURE 65. The Structure of an adaptive feedforward-based control for CDPR with an ISP controller.

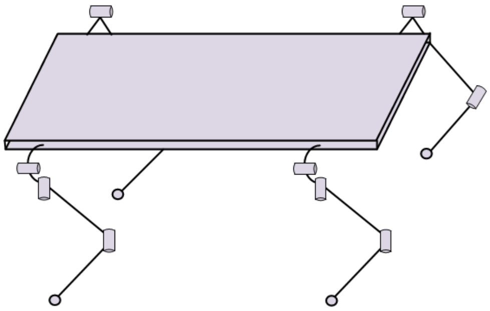

FIGURE 66. The structure of parallel quadruped robot based on serial leg.

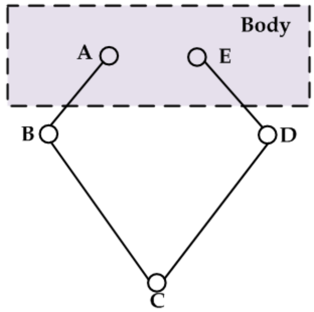

FIGURE 67. The 2 DOF parallel leg mechanism.

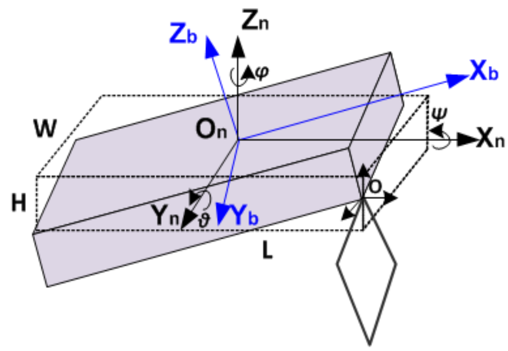

FIGURE 68. The Illustration of coordinate systems and the single rigid body model.

Numerical models of a CDPR with both flexible and stiff cables show the performance and resilience of the suggested controller [75].

J. PARALLEL QUADRUPED ROBOT

The structure of quadruped robots consists of two main components: the torso and the limbs. The limbs are designed with a 3 DOF serial mechanism, arranged from bottom to top as foot-ankle-calf-knee-thigh-hip-torso. After simplification, the quadruped robot with this leg configuration can be attained, as depicted in Figure (66) [76].

The parallel configuration is better suited for small quadruped robots with restricted actuator output power as it overcomes the natural disadvantages of the serial configuration. An example of a quadruped robot with a parallel leg structure is the Stanford Doggo. This robot uses a coaxial parallel instrument and a quasi-direct drive actuator to achieve excellent vertical jumping agility.

However, the quasi-direct drive actuator is expensive and difficult to control, making it unsuitable for large-scale promotion. Additionally, the supportive coaxial mechanism is incompatible with installing the lower-cost steering engine [76].

The Stanford Doggo's parallel leg structure separates the coaxial mechanism, displays the actuators horizontally, and designs a parallel leg mechanism, as illustrated in Figure (67) [76].

1) DYNAMICS OF PARALLEL QUADRUPED ROBOT

The diagram in Figure (68) shows the coordinates of the robot systems. The expressions $\{O_n - x_n y_n z_n\}$ and $\{O_b - x_b y_b z_b\}$ unequivocally denote the world and body coordinates, respectively. The symbols ψ, θ, and ϕ unambiguously represent the roll, pitch, and yaw angles, while R unyieldingly signifies the rotation matrix of the body frame explained in the inertial frame.

$$R = R_z(\psi) R_y(\theta) R_x(\phi) \tag{70}$$

The lower leg rod's design includes carbon to decrease leg mass and inertia significantly. The actuator is strategically placed near the base to concentrate the most mass in the robot body. The assumption is that the ground reaction force (GRF) is the sole external force acting on the feet and that the robot's pitch and roll velocity are negligible. Under these conditions, the GRFs can be expressed as a function of the body base's linear and angular acceleration. The dynamic model is formulated as follows:

$$[\mathrm{A}]\,[\mathrm{x}] = [\mathrm{b}] \begin{bmatrix} \mathrm{I}_3 & \cdots & \mathrm{I}_3 \\ \mathrm{r}_1\times & \cdots & \mathrm{r}_\mathrm{i}\times \end{bmatrix} \begin{bmatrix} \mathrm{F}_{\mathrm{leg},1} \\ \cdots \\ \mathrm{F}_{\mathrm{leg},\mathrm{i}} \end{bmatrix} = \begin{bmatrix} \mathrm{m}(\ddot{\mathrm{x}}^{\mathrm{d}}_{\mathrm{com}} + \mathrm{g}) \\ \mathrm{I}_\mathrm{g}\dot{w}^{\mathrm{d}}_{\mathrm{b}} \end{bmatrix} \tag{71}$$

The given equation (69) describes the relationship between various factors involved in the dynamics of a robot. It includes the mass m and inertia $\mathrm{I_g}$ of the robot, the force of gravity g, the relative position matrix of the $\mathrm{i^{th}}$ leg r, and the desired angular acceleration of the robot's base $\ddot{\mathrm{x}}^{\mathrm{d}}_{\mathrm{com}}$ and the acceleration of the center of mass (CoM) [77].

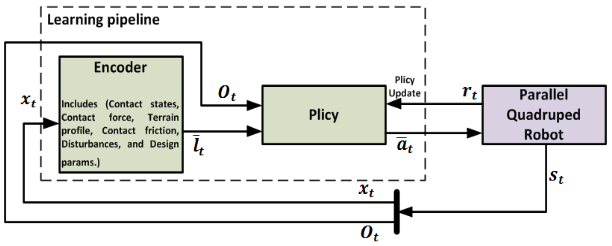

FIGURE 69. The Model-free Reinforcement Learning pipeline for parallel quadruped robot.

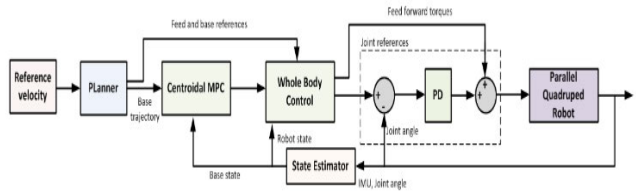

FIGURE 70. Parallel quadruped robot model-based controller.

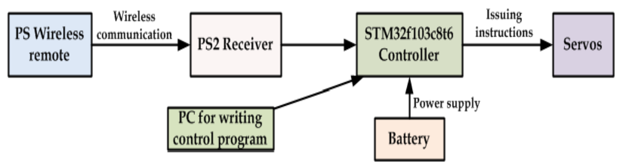

FIGURE 71. The prototype of the control system.

2) CONTROL SCHEMES FOR PARALLEL QUADRUPED ROBOT

This part will briefly discuss the most important control strategies used for motion control of a Parallel quadruped robot, where designing the controller for a parallel quadruped robot to carry out different operations is challenging. These controllers are Learning-Based Control, Model-based Optimal Control, The STM32f103c8t6 Minimum Core Board Control, Adaptive Control, and Optimized Fuzzy Adaptive PID Control.

a: LEARNING-BASED CONTROL

In 2024, Bjelonic et al. [78] introduced a design optimization framework to co-optimize a parallel elastic knee joint and locomotion controller for quadruped robots. They aimed to minimize human intuition by training a design-conditioned policy using model-free Reinforcement Learning. To achieve this, they utilized Bayesian Optimization to identify the best design. Furthermore, they rigorously evaluated the optimized design and controller in real-world experiments across various terrains, as shown in Figure (69), Where the distribution of a_t trained on the observation O_t and gives a reward r_t.

The results demonstrate that the new system enhances the robot's torque-square efficiency by 33% compared to the baseline while reducing the maximum joint torque by 30% without compromising tracking performance. The improved design led to an 11% longer operation time on flat terrain [78].

b: MODEL-BASED OPTIMAL CONTROL

Aractingi [79] is developing Model learning-based controllers for two robots: the lightweight quadruped robot Solo-12 and the heavier Mini-Cheetah. The controllers provide joint angle targets to a PD controller, which outputs the necessary torques, as shown in Figure (70). Their main goal is to enable the robots to follow a user-defined velocity command during locomotion. The team successfully implemented the learned policies from simulation to the actual robots, and they could run the robots in outdoor environments under very challenging conditions. However, they encountered difficulties during the learning process in collecting accurate simulation data that represents the natural system, learning the appropriate behaviour that can be safely deployed on a robot, and adapting the learned material to two different platforms with varied complexity and difficulty levels.

3) THE STM32F103C8T6 MINIMUM CORE BOARD CONTROL

Lu et al. [76] designed a quadruped parallel robot by analyzing the inverse kinematics tacking two-degree-of-freedom parallel legs, which were implemented using a 3D printer, reducing the weighted load and enhancing communication accuracy. The horizontal layout of the driving end was assumed. The trajectory of the foot-end was designed to control the gait of the quadruped robot's four legs during trotting, standing-up, taking-off, and walking. Experiments on a prototype platform [76] confirmed the effectiveness of the foot-end trajectory and the gait stability.

Figure (71) shows that the controller is entirely open source so that any preferred functionality can be counted. The mechanical structure is designed using SolidWorks software, and the parts are manufactured through 3D printing [76].

a: ADAPTIVE CONTROL

In 2022, L. Wang et al. [77] successfully implemented dynamic locomotion for a parallel quadruped robot with symmetric legs and an assertive actuator. Subsequently, they confidently proposed a quick and dependable method established on generalized least squares to estimate terrain parameters by combining body, leg, and contact information.

The quadratic program (QP) method within virtual model control (VMC) allowed us to achieve the optimal foot force for terrain adaptation, as illustrated in Figure (72).

The QP optimization considered the limitations of the friction cone and joint motor assessed. Then, it was translated into joint torques using Jacobian via the optimal solution. Throughout this process, a quick method for estimating the complete terrain information was suggested to maintain balance in the robot's posture [77].

Adaptive control is crucial for legged robots to achieve effective locomotion in complex terrain. Critical components

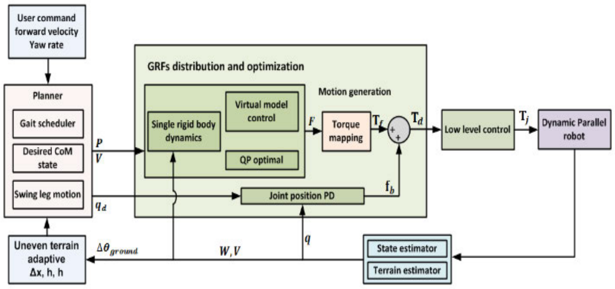

FIGURE 72. The Block diagram of a quadruped parallel robot with controller.

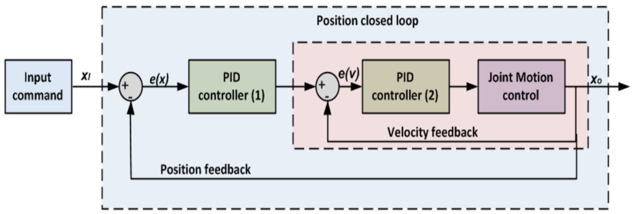

FIGURE 73. Cascade PID controller control block diagram.

of adaptive control include estimating the unknown terrain environment and implementing an online adjustment strategy [77].

The results were gathered using simulation as well as indoor and outdoor experiments. These results showed that the robot has a powerful adaptive ability on uneven terrain and reliable disturbance rejection, which proves the effectiveness and robustness of the proposed method.

b: OPTIMIZED FUZZY ADAPTIVE PID CONTROL

Li et al. [80] utilized the moth flame optimization algorithm and particle swarm optimization algorithm, and the sparrow search algorithm to optimize the cascade proportional–integral–derivative (PID) control system for a parallel quadruped robot. They compared this with the moth flame optimization algorithm and particle swarm optimization algorithm. Additionally, they implemented an improved fuzzy adaptive PID control system to ensure the robot's stable operation. They implemented a cascade PID controller to regulate the robot joint motors. The first closed-loop controls the rotation to match the desired velocity trajectory with minimal error. The second loop of the PID controller is position-closed, as shown in Figure (73).

The outer loop's output serves as the inner loop's input. The inner loop controls the parameters of the motor and sends feedback signals for the motor's angular displacement and velocity to both the external and inner loops. [80]. The fuzzy adaptive PID controller allows the PID controller parameters to adjust adaptively during system operation, which helps the control system achieve higher precision for better controller. The block diagram of controller system is shown in Figure (74).

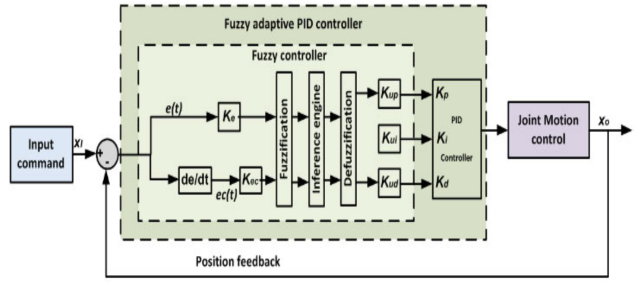

FIGURE 74. The Fuzzy adaptive PID controller control block diagram.

For the PID control cascading, the Sparrow Search Algorithm (SSA) optimizes the six parameters. Despite its high precision, the set objective cannot be attained [80].

In this study, numerical simulations have been implemented to verify the effectiveness of proposed controller. The presented results show that the quadruped bionic robot's movement in terms of displacement and velocity was more accurate and stable when using fuzzy adaptive PID controller systems optimized by the sparrow search algorithm, compared to cascade PID control systems and compared to both the moth flame optimization algorithm and particle swarm optimization algorithm. The simulation results confirmed that the parallel five-link, 8 DOF quadruped robot and its control system offer a reliable solution for operating a quadruped robot [80]. The fuzzy adaptive PID controller has been unequivocally proven to be more effective than controlling the joint motor with the cascade PID controller, providing a solid conclusion to their research.

The report of most above reviewed researches including their comparative control performances in parallel robots is summarized in Table 1.

III. RECOMMENDATIONS

For future extension of this study, the following recommendations can be pursued:

1. One can recommend to conduct another survey which focuses on parallel robots specialized in medical applications. The high precision is the criterion used for evaluating the performance of medical parallel robots, which are directly related to human being life.

2. Another suggestion of this study is to review underwater parallel robots. In such robots, the dynamic model needs deep analysis due to water environment.

3. One can conduct another survey which highlight the challenging problems encountering the implementation of controlled parallel robots in real environment [81], [82], [83], [84], [85], [86], [87].

IV. CONCLUSION

This paper investigates various control strategies designed for different types of parallel robots. The general concepts of controllers and their configurations are briefly discussed.

TABLE 1. Comparative table of different control strategies applied to parallel robots.

No of ref.	Robot type	Controller type	Performance Comparative Evaluation
17, 18	**Delta Parallel robot**	Augmented Nonlinear PD Control (ANPD)	The study showed that the proposed ANPD has better tracking error accuracy compared to APD and NANPD.
19		Identification – Based Control	The hybridization of SMC with ANN has considerably improved the tracking error accuracy.
20		Image-Based Control used three controller: leg-direction-based visual servoing, line-based visual servoing, and image moment visual servoing,	The image moment visual servoing used in this study improved tracking error performance by 45.3% than leg-direction-based visual servoing and by 36.8% than line-based visual servoing.
21		Lagrangian Formulation-Based Control	The article developed control design based on Lagrangian multipliers for Delta robot to achieve satisfactory error tracking performance.
14		Hedge Algebras (HA) - Based Control	The tracking performance using HA-based controller outperforms that based on FLC, and PID controller.
15		B-Spline Neural Network Control (BSNN)	Combining PD controller with BSNN led to improve the error tracking performance.
22		Fuzzy Logic Control	The proposed IT2-FLC gives less tracking error compared to T1-FLC.
13		Fuzzy Logic based Neural Network Control	Combining IT2FLC with ANN has significantly enhanced the tracking error accuracy.
23		Adaptive Robust Control	Optimization of the adaptive control based on FL system lead to robust controller with more practical and economical characteristics.
24		Robust $\mathbf{H}_{\infty}$ Control	Combing robust H_{∞} controller with PID controller could improve tracking error performance.

TABLE 1. *(Continued.)* **Comparative table of different control strategies applied to parallel robots.**

25	**2 DOF - Parallel Robot**	Fault Tolerant Control (FTC)	Proposed FTC with AST-NITSM to improve the error tracking performance.
27		Observers - Based Control	The results of this research showed that DE controllers significantly reduced tracking error performance.
28		Sliding Mode-Based on Backstepping Control (SMC-BS)	The proposed SMC-BS gives better transient characteristic compared to SMC, CTC, and PID Controllers.
26 **29**		Nonlinear Dual Mode Adaptive Control	The proposed Nonlinear Dual Mode Adaptive Control could significantly improve the tracking error accuracy and give faster response as compared to both feed forward controller and PD controllers.
34	**3 DOF - Parallel Robot**	Genetic Algorithm (GA) Optimized PID Control	Optimization of the PID controller based on GA optimization led to improving tracking error performance compared to classical PID controller.
31		Cooperative Control	The proposed Cooperative controller gives better transient characteristics and tracking error performance w.r.t PID Controller.
37		Fuzzy PID controller	The results showed that fuzzy logic PID controller significantly reduced the tracking error compared to conventional PID controller.
32		Fuzzy- Based PID Control	Combing PID controller with Type-II Fuzzy system has improved the tracking error performance.
35 **38**		Interval Type-2 Fuzzy Logic Control	The proposed Type-2 FLC gives less tracking error compared to Type-1 FLC.
42	**4 DOF - Parallel**	Synchronous PD Control Based on a Time-Delay Estimator (SPD-TDE)	-The article developed SPD-TDE control design for 4 DOF parallel robot to achieve satisfactory error tracking performance as compared to PID controller.

TABLE 1. ***(Continued.)*** **Comparative table of different control strategies applied to parallel robots.**

45	R4 Redundantly Parallel Robot	Nonlinear Model Predictive Control	-The proposed Nonlinear Model Predictive Control could significantly improve the tracking error accuracy and give faster response as compared to PD controllers.
41		Synchronous Sliding Mode Control (SSMC)	The proposed SSMC gives better transient characteristic compared to SMC, and PID Controllers.
43		fault-tolerant synchronous sliding mode	The tracking performance using Color/Observer – Based Sliding Mode Control outperforms that based on SSMC, and PID controllers.
40		$\mathbf{L_1}$ Adaptive Control	Better tracking error is obtained with proposed L_1-adaptive controller as compared to PD controller.
46		Adaptive Control	The study showed that Extended $\mathbf{L_1}$ adaptive better enhances the tracking error transient performances w.r.t. conventional $\mathbf{L_1}$ adaptive controller.
47		Adaptive Terminal Sliding Mode Control	The article developed Adaptive TSM to achieve satisfactory error tracking performance as compared to TSM controller.
48 **52**		Dual-Space Feedforward Control	The developed dual-space feed-forward controller improved the accuracy of tracking and provided smoother with less peak overshoot response as compared to feed-forward controller.
50		Dual-Space Feedforward Control in the Cartesian Space	The performance of proposed Dual-Space feed-forward controller outperforms that based on feed-forward controller in the Cartesian space.
49		Dual Mode Adaptive Control (DMAC)	Proposed DMAC to improve the error tracking performance improves the error tracking performance with a maximum acceleration of 100G as compared to dual-space feedforward controller.

TABLE 1. ***(Continued.)*** **Comparative table of different control strategies applied to parallel robots.**

53 **55**	5 R Parallel Robot	Adaptive Control	The results of this research showed that adaptive controller significantly reduced tracking error performance as compared to PD controller.
58		Optimal PID Control	GA-optimized PID controller yields better tracking error performance compared to non-optimized, PSO-optimized and DE-optimized PID controllers.
59		Anti-Windup Based PID Control	The proposed Anti-windup based on PID controller gives better transient characteristic for both Joint and Cartesian spaces compared to PID Controller.
60		Feedback PID Control	The tracking performance using Feedback PID control outperforms that based on PD and PID controllers.
63		PLC – Based Control Architecture	The proposed PLC–Based Control improved the trajectory tracking error up to six motion axes.
64	6 DOF Parallel Robot (HEXA Robot)	Fuzzy PID Control	The proposed Fuzzy-PID control gives better transient characteristic compared to PID Controller.
65		Adaptive Position-Force Control	The results of this research showed that adaptive Position-force controller significantly reduced tracking error as compared to PI controller.
61		Robust Nonlinear Adaptive Control	The designed robust nonlinear adaptive control design for HEXA robot could achieve satisfactory error tracking performance as compared to PID adaptive-robust control.
70	Cable-Driven Parallel Robot	Brain Emotional Learning-Based Intelligent Control	Proposed Brain Emotional Learning-Based Intelligent Control to improve the error tracking performance.
71		Nonlinear Model Predictive Control (NMPC)	The proposed NMPC controller could significantly improve the tracking error accuracy for both translation errors and

TABLE 1. ***(Continued.)*** **Comparative table of different control strategies applied to parallel robots.**

			orientation errors compared to linear MPC controllers.
67		Fuzzy Logic – Based Sliding Surface Control (FL-BSSC)	Combining FL-BSSC with GOA (Grasshopper Optimization Algorithm) improved the tracking error performance.
69		Dual-Space Feedforward Control	The developed Dual-Space Feedforward Control has achieved satisfactory error tracking performance as compared to Dual-Space Control.
73		Rise Feedback Control	Developed Rise Feedback Control design for cable-Driven Parallel robot to achieve satisfactory error tracking performance as compared to PID, and sliding mode controllers.
75		Robust Fault-Tolerant Control (RFTC)	The proposed RFTC could successfully give satisfactory performance for CDP robot in the presence of actuator fault and model uncertainties.
76		Adaptive Passivity-Based Control	The study concluded that the adaptive passivity-based control improved the tracking errors accuracy as compared to both unconstrained attitude parameters Euler-angle, and The special Orthogonal Group SO(3)-based controllers.
80		Model-based Optimal Control (M-BOC)	The proposed M-BOC improved he error tracking trajectory performance.
78	**Parallel Quadruped Robot**	Adaptive Control	The article developed Adaptive Control to achieve satisfactory error tracking performance as compared virtual model control (VMC).
81		Optimized Fuzzy Adaptive PID Control	The developed optimized fuzzy adaptive PID control design for Parallel Quadruped robot to achieve better tracking error as compared to PID, and fuzzy adaptive PID controllers.

Additionally, the dynamic model of each parallel robot considered in this study has been presented. This research covers most of the control strategies utilized in managing parallel robots. The proposed literature review highlights a range of controllers, making it useful for those who are new to the field of parallel robotics. Control researchers can identify and address the gaps in control methods that have not been explored in this study. In order to extend this study, one may valid conduct another review study to highlight the practical challenges in implementing the various types of parallel robots.

TABLE 2. **Units for magnetic properties.**

Symbol	Definition
x_d	the desired joint coordinates
θ_d	the desired joint trajectories
$\tilde{u}$	The H_∞ controller output
u	The torque control vector
θ	the vector of joint coordinates
e	The error
$\dot{e}$	The error derivative
τ	the driving torque
τ_{PD}	The PD control law
τ_{NN}	The IT2FNN control law
x, y, z	the Cartesian
x_d, y_d, z_d	The desired Cartesian
$\theta_{1d}, \theta_{2d}, \theta_{3d}$	The desired joint space
θ_i	The joint i space
e_{θ_i}	the joint i tracking error
$\hat{\sigma}$	The output of the BSNN
$q, \dot{q}$ and $\ddot{q}$	the vectors of positions, velocities and accelerations respectively
$q_d, \dot{q}_d$ and $\ddot{q}_d$	the desired trajectories of positions, velocities and accelerations respectively
$\breve{q}$	The difference between the desired and the actual vectors
x_d	the desired joint coordinates
τ	the driving torque
$\ddot{x}_d$	the desired joint acceleration
Δq	The difference between the desired and actual position vector
K_{ffc}	The best gains of the feedforward controller
K_{ffj}	The feedforward gain, the range
θ_d	the desired joint trajectories
θ	the vector of joint coordinates
K_p	The proportional gain
K_d	The derivative gain
K_i	The integral gain
q_m	the vectors of positions
η	the Actuator torque

APPENDIX
NOMENCLATURE

See Table 2.

REFERENCES

[1] A. Deabs, F. R. Gomaa, and K. Khader, "Review article parallel robot," *J. Eng. Sci. Technol. Rev.*, vol. 14, no. 6, pp. 10–27, 2021.

[2] X.-J. Liu and J. Wang, *Parallel Kinematics Type, Kinematics, and Optimal Design*. New York, NY, USA: Springer, 2014, pp. 3–22.

[3] S. Briot and W. Khalil, *Dynamics of Parallel Robots From Rigid Bodies To Flexible Elements*, vol. 35. Cham, Switzerland: Springer, 2015.

[4] Y. D. Patel and P. M. George, "Parallel manipulators applications—A survey," *Modern Mech. Eng.*, vol. 2, no. 3, pp. 57–64, Jan. 2012.

[5] A. Arora and A. Aggarwal, "A review: Parallel robot in robot assisted surgery," in *Proc. Int. Conf. Advance Res. Innov.*, 2014, pp. 580–584.

[6] A. T. Azar, Q. Zhu, A. Khamis, and D. Zhao, "Control design approaches for parallel robot manipulators: A review," *Int. J. Model., Identificat. Control*, vol. 28, no. 3, p. 199, 2017.

[7] S. Qian, B. Zi, W. Shang, and Q. Xu, "A review on cable-driven parallel robots," *Chin. J. Mech. Eng.*, vol. 31, no. 1, pp. 1–11, 2018.
[8] M. Ratiu and D. M. Anton, "A brief overview of parallel robots and parallel kinematic machines," *IOP Conf. Ser., Mater. Sci. Eng.*, vol. 898, Jul. 2020, Art. no. 012007.
[9] V. E. Abarca and D. A. Elias, "A review of parallel robots: Rehabilitation, assistance, and humanoid applications for neck, shoulder, wrist, hip, and ankle joints," *Robotics*, vol. 12, no. 5, p. 131, Sep. 2023.
[10] R. Kelaiaia, A. Chemori, A. Brahmia, A. Kerboua, A. Zaatri, and O. Company, "Optimal dimensional design of parallel manipulators with an illustrative case study: A review," *Mechanism Mach. Theory*, vol. 188, Oct. 2023, Art. no. 105390.
[11] M. Russo, D. Zhang, X.-J. Liu, and Z. Xie, "A review of parallel kinematic machine tools: Design, modeling, and applications," *Int. J. Mach. Tools Manuf.*, vol. 196, Mar. 2024, Art. no. 104118.
[12] Z. Shareef, "Path planning and trajectory optimization of delta parallel robot," Ph.D. dissertation, Dept. Mech. Eng., Paderborn Univ., Karachi, Pakistan, May 2015.
[13] X. Lu, Y. Zhao, and M. Liu, "Self-learning interval type-2 fuzzy neural network controllers for trajectory control of a delta parallel robot," *Neurocomputing*, vol. 283, pp. 107–119, Mar. 2018.
[14] T.-L. Bui, T.-H. Nguyen, and X.-T. Nguyen, "A controller for delta parallel robot based on Hedge algebras method," *J. Robot.*, vol. 2023, pp. 1–20, Jan. 2023, doi: 10.1155/2023/2271030.
[15] J. M. Escorcia-Hernández, H. Aguilar-Sierra, O. Aguilar-Mejía, A. Chemori, and J. H. Arroyo-Núñez, "An intelligent compensation through B-spline neural network for a delta parallel robot," in *Proc. 6th Int. Conf. Control, Decis. Inf. Technol. (CoDIT)*, Paris, France, Apr. 2019, pp. 361–366.
[16] Y.-L. Kuo, "Mathematical modeling and analysis of the delta robot with flexible links," *Comput. Math. With Appl.*, vol. 71, no. 10, pp. 1973–1989, May 2016.
[17] A. J. Humaidi and A. I. Abdulkareem, "Design of augmented nonlinear PD controller of Delta/Par4-like robot," *J. Control Sci. Eng.*, vol. 2019, pp. 1–11, Jul. 2019, doi: 10.1155/2019/7689673.
[18] A. J. Humaidi, A. A. Oglah, S. J. Abbas, and I. K. Ibraheem, "Optimal augmented linear and nonlinear PD control design for parallel robot based on PSO tuner," *Int. Rev. Model. Simul. (IREMOS)*, vol. 12, no. 5, p. 281, Oct. 2019.
[19] A. Zhao, A. Toudeshki, R. Ehsani, J. H. Viers, and J.-Q. Sun, "Evaluation of neural network effectiveness on sliding mode control of delta robot for trajectory tracking," *Algorithms*, vol. 17, no. 3, p. 113, Mar. 2024.
[20] M. Zhu, A. Chriette, and S. Briot, "Control-based design of a DELTA robot," in *Proc. 23rd CISM IFTOMM Symp. Robot Design, Dyn. Control*, Sapporo, Japan, Sep. 2020, pp. 1–8.
[21] F.-S. Lee and C.-I Lin, "Controller design for a delta robot using Lagrangian multipliers," *Res. Square*, vol. 1, Sep. 2021.
[22] X.-G. Lu, M. Liu, and J.-X. Liu, "Design and optimization of interval type-2 fuzzy logic controller for delta parallel robot trajectory control," *Int. J. Fuzzy Syst.*, vol. 19, no. 1, pp. 190–206, Feb. 2017.
[23] L. Wu, R. Zhao, Y. Li, and Y.-H. Chen, "Optimal design of adaptive robust control for the delta robot with uncertainty: Fuzzy set-based approach," *Appl. Sci.*, vol. 10, no. 10, p. 3472, May 2020.
[24] M. Rachedi, B. Hemici, and M. Bouri, "Design of an H_∞ controller for the delta robot: Experimental results," *Adv. Robot.*, vol. 29, no. 18, pp. 1165–1181, Sep. 2015.
[25] M. Mazare, M. Taghizadeh, and P. Ghaf-Ghanbari, "Fault-tolerant control based on adaptive super-twisting nonsingular integral-type terminal sliding mode for a delta parallel robot," *J. Brazilian Soc. Mech. Sci. Eng.*, vol. 42, no. 8, p. 443, Aug. 2020, doi: 10.1007/s40430-020-02510-3.
[26] A. Chemori, G. S. Natal, and F. Pierrot, "Control of parallel robots: Towards very high accelerations," presented at the 10th Int. Multi-Conf. Syst., Signals Devices (SSD), Hammamet, Tunisia, Mar. 2013.
[27] G. S. Natal, A. Chemori, and F. Pierrot, and O. Company, "An experimental comparison of state observers for the control of a parallel anipulator without velocity measurements," in *Proc. IEEE/RSJ Int. Conf. Intell. Robots Syst.*, Oct 2010.
[28] E. Litim, "Trajectory planning and motion control schemes for 2DoF planar parallel manipulator biglide type with elastic joints: A comparative study," *Przegląd Elektrotechniczny*, vol. 1, no. 8, pp. 90–97, Aug. 2021.
[29] G. S. Natal, A. Chemori, and F. Pierrot, "Nonlinear control of parallel manipulators for very high accelerations without velocity measurement: Stability analysis and experiments on Par2 parallel manipulator," *Robotica*, vol. 34, no. 1, pp. 43–70, Jan. 2016.
[30] S. A. Rad, M. G. Tamizi, A. Mirfakhar, M. T. Masouleh, and A. Kalhor, "Control of a two-DOF parallel robot with unknown parameters using a novel robust adaptive approach," *ISA Trans.*, vol. 117, pp. 70–84, Nov. 2021.
[31] Q. Huang, G. He, G. Feng, and B. Ding, "A novel cooperative control strategy for three-degree-of-freedom pneumatic parallel mechanism," *Actuators*, vol. 13, no. 3, p. 89, Feb. 2024, doi: 10.3390/act13030089.
[32] J. Tavoosi and F. Mohammadi, "A 3-PRS parallel robot control based on fuzzy-PID controller," in *Proc. 6th Int. Conf. Control, Instrum. Autom. (ICCIA)*, Sanandaj, Iran, Oct. 2019.
[33] M. Díaz-Rodríguez, A. Valera, V. Mata, and M. Valles, "Model-based control of a 3-DOF parallel robot based on identified relevant parameters," *IEEE/ASME Trans. Mechatronics*, vol. 18, no. 6, pp. 1737–1744, Dec. 2013.
[34] L. Sheng and W. Li, "Optimization design by genetic algorithm controller for trajectory control of a 3-RRR parallel robot," *Algorithms*, vol. 11, no. 1, p. 7, Jan. 2018.
[35] H. T. Najem, "Optimal fuzzy logic control for 3-RRR planar parallel manipulator," M.S. thesis, Dept. Control Syst. Eng., Univ. Technol. Iraq, Baghdad, Iraq, 2019.
[36] N. C. Ruiz-Hidalgo, A. Blanco-Ortega, A. Abúndez-Pliego, J. Colín-Ocampo, and M. Arias-Montiel, "Design and control of a novel 3-DOF parallel robot," in *Proc. Int. Conf. Mechatronics, Electron. Automot. Eng. (ICMEAE)*, Cuernavaca, Mexico, Nov. 2016, pp. 66–71.
[37] T. Li, M. Gong, K. Hu, L. Zhao, and B. Zhao, "A novel 3-DOF translational parallel robot and its fuzzy controller design," *J. Intell. Fuzzy Syst.*, vol. 41, no. 3, pp. 4211–4224, Oct. 2021.
[38] A. J. Humaidi, H. T. Najem, A. Q. Al-Dujaili, D. A. Pereira, I. K. Ibraheem, and A. T. Azar, "Social spider optimization algorithm for tuning parameters in PD-like interval type-2 fuzzy logic controller applied to a parallel robot," *Meas. Control*, vol. 54, nos. 3–4, pp. 303–323, Mar. 2021.
[39] J. Wu and Z. Yin, "A novel 4-DOF parallel manipulator H4, parallel manipulators, towards new applications," I-Tech Educ. Publishing, Vienna, Austria, pp. 405–448, Apr. 2008, doi: 10.5772/5441.
[40] M. Bennehar, A. Chemori, and F. Pierrot, "L1 adaptive control of parallel kinematic manipulators: Design and real-time experiments," in *Proc. IEEE Int. Conf. Robot. Autom. (ICRA), Washington State Conv. Center Seattle*, Washington, DC, USA, May 2015, pp. 1587–1592.
[41] D. T. Tran, T. N. Nguyen, M. T. Nguyen, V. T. Ngo, and H. L. Le, "Synchronous sliding mode control for a 4-DOF parallel manipulator in practice," *J. Tech. Educ. Sci.*, vol. 18, no. 3, pp. 1–13, Aug. 2023.
[42] D. T. Tran, T. N. Nguyen, X. T. Nguyen, and D. M. Nguyen, "Synchronous PD control using a time delay estimator for a four-degree-of-freedom parallel robot in practice," *Machines*, vol. 11, no. 8, p. 831, Aug. 2023.
[43] D. T. Tran, N. T. Nha, N. Van Thuyen, L. H. Lam, and K. K. Ahn, "A fault-tolerant synchronous sliding mode control for a 4-DOF parallel manipulator with uncertainties and actuator faults," *Int. J. Control, Autom. Syst.*, vol. 22, no. 4, pp. 1313–1323, Apr. 2024.
[44] R. J. Escarabajal, J. L. Pulloquinga, V. Mata, Á. Valera, and M. Díaz-Rodríguez, "Model-based control of a 4-DOF rehabilitation parallel robot with online identification of the gravitational term," *Sensors*, vol. 23, no. 5, p. 2790, Mar. 2023.
[45] R. Kouki, A. Chemori, and F. Bouani, "A new fast NMPC scheme for parallel kinematic manipulators: Design and real-time experiments," in *Proc. Int. Conf. Signal, Control Commun. (SCC)*, Hammamet, Tunisia, Dec. 2019.
[46] M. Bennehar, A. Chemori, S. Krut, and F. Pierrot, "Adaptive control of parallel manipulators: Design and real-time experiments," in *Title of His Published Book Parallel Manipulators: Design, Applications and Dynamic Analysis*. Hauppauge, NY, USA: Nova Science Inc., 2016, ch. 1, pp. 1–30.
[47] M. Bennehar, G. El-Ghazaly, A. Chemori, and F. Pierrot, "A novel adaptive terminal sliding mode control for parallel manipulators: Design and real-time experiments," in *Proc. IEEE Int. Conf. Robot. Autom. (ICRA)*, Singapore, May 2017, pp. 6086–6092.
[48] G. S. Natal, A. Chemori, and F. Pierrot, "Dual-space adaptive control of redundantly actuated parallel manipulators for extremely fast operations with load changes," in *Proc. IEEE Int. Conf. Robot. Autom.*, Saint Paul, MN, USA, May 2012, pp. 253–258.
[49] G. Sartori Natal, A. Chemori, and F. Pierrot, "Dual-space control of extremely fast parallel manipulators: Payload changes and the 100G experiment," *IEEE Trans. Control Syst. Technol.*, vol. 23, no. 4, pp. 1520–1535, Jul. 2015.

[50] M. Bennehar, A. Chemori, S. Krut, and F. Pierrot, ''Continuous closed form trajectories generation and control of redundantly actuated parallel kinematic manipulators,'' in *Proc. IEEE 11th Int. Multi-Conf. Syst., Signals Devices (SSD)*, Feb. 2014, pp. 1–6.

[51] G. S. Natal, A. Chemori, M. Michelin, and F. Pierrot, ''A dual-space feed-forward PID control of redundantly actuated parallel manipulators with real-time experiments,'' in *Proc. IFAC Conf. Adv. PID Control*, Brescia, Italy, Mar. 2012, p. 6.

[52] H. A.-H. Hussein, ''Adaptive controller for R4 parallel robot,'' M.S. thesis, Dept. Control Syst. Eng., Univ. Technol., Baghdad, Iraq, 2019.

[53] A. J. Humaidi and H. A. Hussein, ''Adaptive control of parallel manipulator in Cartesian space,'' in *Proc. IEEE Int. Conf. Electr., Comput. Commun. Technol. (ICECCT)*, Feb. 2019, pp. 1–8.

[54] G. Pagis, N. Bouton, S. Briot, and P. Martinet, ''Design of a controller for enlarging parallel robots workspace through type 2 singularity crossing,'' in *Proc. IEEE Int. Conf. Robot. Autom. (ICRA)*, Hong Kong, May 2014, pp. 4249–4255.

[55] F. A. Lara-Molina and E. H. Koroishi, ''Kinematic analysis of planar 5R symmetrical parallel manipulator using an interval approach,'' in *Proc. Latin Amer. Robot. Symp. (LARS), Brazilian Symp. Robot. (SBR) Workshop Robot. Educ. (WRE)*, Brazil, Nov. 2020, pp. 1–6.

[56] M. Gohari, Z. Soleymanian, F. Foroutan, and M. Tahmasebi, ''Design controller and fibrication of 5R parallel robot for biopsy operation,'' *Int. J. Appl. Math., Comput. Sci. Syst. Eng.*, vol. 4, pp. 93–97, Dec. 2022, doi: 10.37394/232026.2022.4.12.

[57] D. K. Sen, A. Yildiz, and O. Kopmaz, ''Optimal design of a five-bar planar manipulator and its controller by using different algorithms for minimum shaking forces and moments for the largest trajectory in a usable workspace,'' *Machines*, vol. 10, no. 11, p. 971, Oct. 2022.

[58] H. Saied, A. Chemori, M. Michelin, M. El-Rafei, C. Francis, and F. Pierrot, ''A redundant parallel robotic machining tool: Design, control and real-time experiments,'' *New Develop. Adv. Robot Control*, vol. 175, pp. 39–79, Jan. 2019.

[59] P. Righettini, R. Strada, F. Cortinovis, F. Tabaldi, J. Santinelli, and A. Ginammi, ''An experimental investigation of the dynamic performances of a high speed 4-DOF 5R parallel robot using inverse dynamics control,'' *Robotics*, vol. 13, no. 3, p. 54, Mar. 2024.

[60] N. Negahbani, H. Giberti, and E. Fiore, ''Error analysis and adaptive-robust control of a 6-DoF parallel robot with ball-screw drive actuators,'' *J. Robot.*, vol. 2016, no. 1, pp. 1–15, 2016.

[61] H. Abdellatif and B. Heimann, ''Advanced model-based control of a 6-DOF hexapod robot: A case study,'' *IEEE/ASME Trans. Mechatronics*, vol. 15, no. 2, pp. 269–279, Apr. 2010, doi: 10.1109/TMECH.2009.2024682.

[62] C. Vaida, D. Pisla, F. Covaciu, B. Gherman, A. Pisla, and N. Plitea, ''Development of a control system for a HEXA parallel robot,'' in *Proc. IEEE Int. Conf. Autom., Quality Test., Robot. (AQTR)*, May 2016, pp. 1–6.

[63] M. Babaiasl, S. H. Mahdioun, A. Azizi, and M. Dehghani, ''Fuzzy PID control of a 6-DOF parallel robot,'' *Echarithm*, Nov. 2020. [Online]. Available: https://mecharithm.com/news/article/fuzzy-pid-control-of-a-6-dof-parallel-robot

[64] L. J. Puglisi, ''Advanced control strategies for a 6 DOF hydraulic parallel robot based on the dynamic model,'' Ph.D. dissertation, Politécnica Univ., Madrid, Spain, 2016.

[65] T. Sun, J. Sun, B. Lian, and Q. Li, ''Sensorless admittance control of 6-DoF parallel robot in human-robot collaborative assembly,'' *Robot. Comput.-Integr. Manuf.*, vol. 88, Aug. 2024, Art. no. 102742.

[66] M. Aghaseyedabdollah, M. Abedi, and M. Pourgholi, ''Interval type-2 fuzzy sliding mode control for a cable-driven parallel robot with elastic cables using metaheuristic optimization methods,'' *Math. Comput. Simul.*, vol. 218, pp. 435–461, Apr. 2024.

[67] M.-T. Vu, K.-H. Hsia, F. F. M. El-Sousy, T. Rojsiraphisal, R. Rahmani, and S. Mobayen, ''Adaptive fuzzy control of a cable-driven parallel robot,'' *Mathematics*, vol. 10, no. 20, p. 3826, Oct. 2022.

[68] J. Lamaury, M. Gouttefarde, A. Chemori, and P.-E. Hervé, ''Dual-space adaptive control of redundantly actuated cable-driven parallel robots,'' in *Proc. IEEE/RSJ Int. Conf. Intell. Robots Syst. (IROS)*, Nov. 2013, pp. 4879–4886.

[69] M. Bajelania, S. A. Khalilpoura, M. I. Hosseinia, H. D. Taghirada, and P. Cardou, ''Model-free joint space controller for fully-constrained cable-driven parallel robots: A bio-inspired algorithm,'' *Int. J. Robot.*, vol. 9, no. 1, pp. 11–19, 2023.

[70] J. C. Santos, M. Gouttefarde, and A. Chemori, ''A nonlinear model predictive control for the position tracking of cable-driven parallel robots,'' *IEEE Trans. Robot.*, vol. 38, no. 4, pp. 2597–2616, Aug. 2022.

[71] S. Abdolshah and E. Shojaei Barjuei, ''Linear quadratic optimal controller for cable-driven parallel robots,'' *Frontiers Mech. Eng.*, vol. 10, no. 4, pp. 344–351, Dec. 2015.

[72] G. Hassan, A. Chemori, L. Chikh, P.-E. Hervé, M. E. Rafei, C. Francis, and F. Pierrot, ''RISE feedback control of cable-driven parallel robots: Design and real-time experiments,'' presented at the 1st Virtual IFAC World Congress, vol. 53, no. 2, Berlin, Germany, Jul. 2020, pp. 8519–8524.

[73] Y. Lu and W. Yao, ''Active fault-tolerant hybrid control integrated with reinforcement learning application to cable-driven parallel robots,'' *Control Eng. Pract.*, vol. 158, May 2025, Art. no. 106277.

[74] S. M. Fazeli, M. Abedi, A. Molaei, M. Hassani, M. A. Khosravi, and A. Ameri, ''Active fault-tolerant control of cable-driven parallel robots,'' *Nonlinear Dyn.*, vol. 111, no. 7, pp. 6335–6347, Dec. 2022.

[75] S. K. Cheah, A. Hayes, and R. J. Caverly, ''Adaptive passivity-based pose tracking control of cable-driven parallel robots for multiple attitude parameterizations,'' *IEEE Trans. Control Syst. Technol.*, vol. 32, no. 1, Jan. 2024.

[76] M. Lu, B. Jing, H. Duan, and G. Gao, ''Design of a small quadruped robot with parallel legs,'' *Complexity*, vol. 2022, no. 1, pp. 1–11, Sep. 2022. [Online]. Available: https://doi.org/10.1155/2022/9663746

[77] L. Wang, L. Meng, R. Kang, B. Liu, S. Gu, Z. Zhang, F. Meng, and A. Ming, ''Design and dynamic locomotion control of quadruped robot with perception-less terrain adaptation,'' *Cyborg Bionic Syst.*, vol. 2022,Feb. 2022, Art. no. 9816495, doi: 10.34133/2022/9816495.

[78] F. Bjelonic, J. Lee, P. Arm, D. Sako, D. Tateo, J. Peters, and M. Hutter, ''Learning-based design and control for quadrupedal robots with parallel-elastic actuators,'' *IEEE Robot. Autom. Lett.*, vol. 8, no. 3, pp. 1611–1618, Mar. 2023.

[79] M. Aractingi, ''Controlling the locomotion of quadruped robots with learning methods,'' Ph.D. dissertation, Insa Toulouse, Univ. Federale Toulouse, Robotics, Dec. 2023.

[80] M. Li, Z. Liu, M. Wang, G. Pang, and H. Zhang, ''Design of a parallel quadruped robot based on a novel intelligent control system,'' *Appl. Sci.*, vol. 12, no. 9, p. 4358, Apr. 2022.

[81] A. J. Humaidi, T. M. Kadhim, S. Hasan, I. K. Ibraheem, and A. T. Azar, ''A generic Izhikevich-modelled FPGA-realized architecture: A case study of printed English letter recognition,'' in *Proc. 24th Int. Conf. Syst. Theory, Control Comput. (ICSTCC)*, Sinaia, Romania, Oct. 2020, pp. 825–830, doi: 10.1109/ICSTCC50638.2020.9259707.

[82] A. K. Aljumaili, R. F. Hassan, E. K. Hamza, and A. J. Humaidi, ''FPGA implementation of lowpass FIR filter using single multiply-accumulate unit with dual-port RAM,'' *J. Eng. Sci. Technol.*, vol. 20, no. 1, pp. 345–361, 2025.

[83] A. J. Humaidi and T. M. Kadhim, ''Spiking versus traditional neural networks for character recognition on FPGA platform,'' *J. Telecommun., Electron. Comput. Eng.*, vol. 10, no. 3, pp. 109–115, Aug. 2018.

[84] A. M. Dalloo, A. J. Humaidi, A. K. Al Mhdawi, and H. Al-Raweshidy, ''Approximate computing: Concepts, architectures, challenges, applications, and future directions,'' *IEEE Access*, vol. 12, pp. 146022–146088, 2024, doi: 10.1109/ACCESS.2024.3467375.

[85] A. M. Dalloo and A. J. Humaidi, ''Optimizing machine learning models with data-level approximate computing: The role of diverse sampling, precision scaling, quantization and feature selection strategies,'' *Results Eng.*, vol. 24, Dec. 2024, Art. no. 103451, doi: 10.1016/j.rineng.2024.103451.

[86] A. M. Dalloo, A. J. Humaidi, A. K. A. Mhdawi, and H. Al-Raweshidy, ''Low-power and low-latency hardware implementation of approximate hyperbolic and exponential functions for embedded system applications,'' *IEEE Access*, vol. 12, pp. 24151–24163, 2024, doi: 10.1109/ACCESS.2024.3364361.

[87] M. L. Muhammed, E. H. Flaieh, and A. J. Humaidi, ''Embedded system design of path planning for planar manipulator based on chaos A* algorithm with known-obstacle environment,'' *J. Eng. Sci. Technol.*, vol. 17, no. 6, pp. 4047–4064, 2022.

SHAYMAA MAHMOOD MAHDI received the B.Sc. degree in computer engineering and the M.Sc. degree in mechatronics engineering from the Department of Control and Systems Engineering, University of Technology-Iraq, Iraq, in 2003 and 2008, respectively. She is currently a Professor with the Engineering College, University of Technology-Iraq. Her research interests include adaptive, nonlinear and intelligent control, optimization, and robotics.

AHMED I. ABDULKAREEM was born in Baghdad, Iraq, in 1978. He received the B.S. degree in computer engineering and the M.S. degree in mechatronics engineering from the University of Technology-Iraq, in 1999 and 2001, respectively, and the Ph.D. degree in automation and mobile robot engineering from Salford University, Manchester, U.K., in 2012.

From 2002 to 2007, he was a Lecturer with the University of Technology-Iraq. Since 2016, he has been an Assistant Professor with the Department of Mechatronics and Robotics Engineering, University of Technology-Iraq, where he has been a Professor, since 2021. He is the author of more than 20 articles. His research interests include automation and mobile robotics, decision-making under risk, evolutionary computations, linear and nonlinear controllers, optimization techniques, artificial intelligence, swarm intelligence, soft computing, and dynamic and static systems.

AMJAD JALEEL HUMAIDI received the B.Sc. and M.Sc. degrees in control engineering from the Al-Rasheed College of Engineering and Science, in 1992 and 1997, respectively, and the Ph.D. degree in control and automation, in 2006. He is currently a Professor with the Engineering College, University of Technology-Iraq. His research interests include adaptive, nonlinear, and intelligent control, optimization, and real-time image processing.

AMMAR K. AL MHDAWI received the Ph.D. degree in electronic and electrical engineering from the Brunel University of London, U.K., and the Postdoctoral degree from Newcastle University, U.K. He is currently a Lecturer in control engineering with De Montfort University, Leicester, U.K. He has substantial engineering experience with over 15 years. His research interests include control systems, robotics, mechatronics, AUV, UAV, AGV, intelligent control, sustainable systems, and interconnected systems.

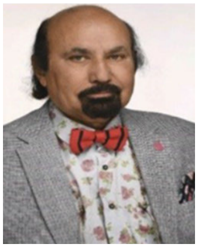

HAMED AL-RAWESHIDY (Senior Member, IEEE) received the B.Eng. and M.Sc. degrees from the University of Technology, Baghdad, in 1977 and 1980, respectively, the master's Diploma degree from Glasgow University, Glasgow, U.K., in 1987, and the Ph.D. degree from Strathclyde University, Glasgow, in 1991. He is currently a Professor in engineering. He was with the Space and Astronomy Research Centre, Iraq; PerkinElmer, USA; Carl Zeiss, Germany; British Telecom, U.K.; and various universities, such as Oxford University, Manchester Metropolitan University, and Kent University. He is also the Director of the Wireless Networks and Communications Centre (WNCC) and the Director of PG Studies (ECE) with the Brunel University of London, U.K. He has published over 370 papers in international journals and refereed conferences. His current research interests beyond 5G and 6G, such as 6G quantum and AI, RIS with quantum and AI, near and far edge, the IoT with AI, radio over fiber for IoT with quantum and AI, and offloading and load balancing with AI. He is a member of several journal editorial boards, such as *Journal of Wireless Personal Communications*. He is an Editor of the first book *Radio Over Fibre Technologies for Mobile Communications Networks*. He has acted as a Guest Editor of the *International Journal of Wireless Personal Communications*.